Tampere University

Ossi Mäkelä

# MEASUREMENT METHOD FOR 2-DIMENSIONAL COORDINATE SYSTEM

Engineering Sciences
Master's of Science Thesis
December 2019

# ABSTRACT

Ossi Mäkelä: Measurement method for 2-dimensional coordinate system
Master's of Science Thesis
Tampere University
Degree Programme in Automation Engineering MSc
December 2019

---

The subject of this Master's of Science Thesis is to study suitability of predefined technologies and development of a measurement system for measuring Cartesian style robot's positioning accuracy within its x/y-plane. The methods currently used for measuring and calibrating robot positioning are based on commercial solutions or measurement systems developed internally. Both of these have their non-beneficial properties that lead to the commissioning of this thesis work. The commercial system provides a high accuracy and repeatability performance but are often costly and difficult or impossible to integrate to the robot system in question. The second mentioned measurement system has much lower building costs but it only measures in one axis at a time and thus, it doesn't see the possible orthogonality errors. This problem was approached with three methodologies covering the theoretical background of the main geometrical error sources, some basics of the theory of measurement uncertainty, evaluation procedure for evaluating suitability of technologies for measuring positioning and developing a measurement system with the selected technology based on the evaluation results. The technologies are evaluated with a scoring system based on criterion that sets a range of requirements for e.g. accuracy performance and other functionality. The goal of this thesis was to develop a low cost, system integrable positioning measurement system and study its performance and usability by comparing it to commercial measurement systems and systems design and developed internally.

After conducting evaluation of the technologies, a camera-based technology was selected for development phase. This technology solution includes a camera and optics that are the robots standard equipment and thus won't add any additional costs. This solution requires a measurement target which is used with the camera to detect motion and algorithms for camera calibration and for calculating motion increments from the captured images. With the combination of camera, optics and the measurement target a value of 55.2 pixels per millimeter was obtained which translates to $17.9\,\mu\mathrm{m} \pm 0.001$-pixel size in the measurement images.

Keywords: robot motion accuracy, accuracy measurement, linear axis, motion accuracy, motion error
The originality of this thesis has been checked using the Turnitin OriginalityCheck service.

# TIIVISTELMÄ

Ossi Mäkelä: Mittausmenetelmä robotin x/y-tason liiketarkkuuden mittaamiseen
Diplomityö
Tampereen yliopisto
Automaatiotekniikan diplomi-insinöörin tutkinto-ohjelma
Joulukuu 2019

---

Tämän diplomityön aiheena on tutkia ennalta määriteltyjen teknologioiden soveltuvuutta karteesisen robotin x/y-tason liiketarkkuuden mittaamiseen sekä kehittää soveltuvimpaan teknologiaan perustuva mittausjärjestelmä. Työn alussa käydään läpi robotin liiketarkkuuteen vaikuttavien geometristen virheläteiden alkuperää sekä mittausteknisen epävarmuuden muodostavat tekijät kirjallisen taustatutkimuksen menetelmin. Työhön on työn tilaajan puolesta määritelty teknologiat, joiden soveltuvuutta mittausjärjestelmän kehittämiseen arvioidaan pisteytystaulukon avulla. Kehitettävälle mittausjärjestelmälle on asetettu toimintakriteerit, joiden pohjalta pisteytystaulukko ja pisteytys on määritelty. Työn tavoitteena oli toteuttaa edullinen robottiin integroitava mittausmenetelmä ja tutkia sen mittaustarkkuutta sekä käyttökelpoisuutta robotin liiketarkkuuden mittaamiseen, vertaamalla tuloksia kaupallisiin mittausjärjestelmiin.

Mittausjärjestelmälle asetettujen toimintakriteihin perustuvan pisteytysjärjestelmän avulla, työn totetutusvaiheeseen valittiin kamerateknologiaan pohjautuva kuvantamismenetelmä, josta kehitetty mittausjärjestelmä koostuu robotin laitteistoon kuuluvasta kamerasta ja optiikasta sekä erillisestä mitta-asteikosta. Työssä suunniteltu ja kehitetty mittausjärjestelmä perustuu kuvantamisalgoritmeihin, jotka mahdollistavat mitta-asteikosta otetuista kuvista robotin liikkeen mittaamisen alipikselitasolla. Mittausjärjestelmän kameralla ja optiikka yhdistelmällä saadaan kuvia, joissa yhden pikselin koko on $17.9\,\mu\mathrm{m} \pm 0.001$

Avainsanat: robotin liiketarkkuus, tarkkuusmittaus, lineaariakseli, liiketarkkus, liikevirhe
Tämän julkaisun alkuperäisyys on tarkastettu Turnitin OriginalityCheck -ohjelmalla.

# PREFACE

This thesis was made during 2018-2019 for Optofidelity Oy. I am greatful to finally get this thesis finished as it has been a challenging task to merge to a job with substantial amount of traveling.

The subject of this Master of Science thesis is based on the idea originally presented by Ari Nevalainen at OptoFidelity Oy. I want to thank Jere Paloniemi from Optofidelity for patience and guidance during the whole thesis process.

This thesis was examined by Dr.David Hästbacka whom also took part by guiding the thesis writing process. I also want to thank Jorma Vihinen from Tampere University for granting access to measurement equipment which were required in the thesis.

In Tampere, 29th December 2019

Ossi Mäkelä

# CONTENTS

# LIST OF FIGURES

# LIST OF TABLES

# LIST OF SYMBOLS AND ABBREVIATIONS

| | |
|---|---|
| $c_0$ | Speed of Light |
| $\overline{x}$ | Arithmetic mean |
| $s$ | Standard deviation |
| $u_A$ | TypeA standard uncertainty |
| $u_B$ | TypeB standard uncertainty |
| $u_C$ | Standard uncertainty of particular measurement |
| $U$ | Expanded standard uncertainty |
| 3-DoF | 3 Degrees of Freedom |
| RSS | Root Sum of Squares |
| JCGM | Joint Commitee for Guides in Metrology |
| CMOS | Complementary metal-oxide-semiconductor |
| CCD | Charge-coupled device |
| PSD | Position Sensitive Detector |
| LED | Light Emitting Diode |
| cpi | counts per inch |
| VCSEL | Vertical-Cavity Surface Emitting Laser |
| ppmm | pixels per millimeter |
| SUD | System Under Development |
| CMM | Coordinate Measuring Machine |
| FOV | Field of View |
| IPR | Intellectuel Property Rights |

# 1 INTRODUCTION

In the field of industrial robotics, the positioning of a robot end-effector, workpiece or any other object on the robot coordinate system is an essential part of a robot application. A vast amount of studies and experiments have successfully been conducted in effort to develop methods to measure robot end-effector position with sufficient accuracy. Many robot manufacturers have their own preferred methods of measuring and presenting robot performance characteristics, but in many cases, the end user has designed an application specific end-effector which may require a specific method of positioning performance measurement. Another motivation that drives engineers to develop new methods to measure positioning, is the increased accuracy requirements in many end user application. The improvement in machining accuracy has made it possible to design and build positioning systems to supply the demand of increasing accuracy requirements. Some of today's positioning systems used in manufacturing and inspection processes such as semiconductor manufacturing, has reached performance characteristics of sub-micron or even nanometer level in precision machining accuracy [3]. This increase in machining accuracy reflects directly to the measurement system performance requirements.

In terms of robot positioning performance, there are many variables in place which can have significant affect to the robot accuracy and repeatability. One of the most essential contributing factor is the design features of the robot's kinematic scheme. In this thesis, a gantry style 3-DoF rectangular Cartesian coordinate robot's positioning performance and error sources are studied. This type of robot's kinematic scheme consists of three linear axes that ideally, are in right angle or perpendicular to each other. Because of the rigid nature of the kinematic scheme, Cartesian robots provide considerably better positioning characteristics compared to robots with other kinematic configurations[20]. The Cartesian style robot is widely utilized in OptoFidelity's customized robot solutions that require a micrometer level positioning performance. The usual tasks of these robot solutions are to perform gestures such as tap and swipe on a touch-screen device that must be performed within micrometer level position error constrains. These demanding constrains require not only high repeatability but also high motion accuracy characteristics.

To measure both repeatability and motion accuracy with the high positioning error constrains, choosing a suitable technology becomes a difficult task. A large variety of technologies have been utilized in robot repeatability and accuracy measurement applications which have a wide range of performance characteristics. To narrow down these possibly suitable technologies, they are compared with respect to the intended applications performance requirements and other pre-defined properties. The technologies to be compared are laser interferometry, laser triangulation, camera-based circle pattern recognition and optical mouse sensor based solution. The list of options were defined by the company's metrology team.

## 1.1 Problem definition

When considering a linear motion stage, whether it's based on a stepper motor and a lead screw, a linear motor and guide rails or some other configuration, a variety of error sources have impact on its positioning performance. It is not an easy task to distinguish different error sources from each other and their individual magnitude of impact to the total error sum. Nevertheless, it is important to be able to measure the amount of error within each position in the robots coordinate

with sufficient accuracy to be able to develop a method of positioning calibration. The robot in question in this thesis is a Cartesian style robot which mechanical construction is illustrated in the figure 1.1. A Cartesian robot is constructed from three perpendicular axes.

***Figure 1.1.*** *Cartesian robot*

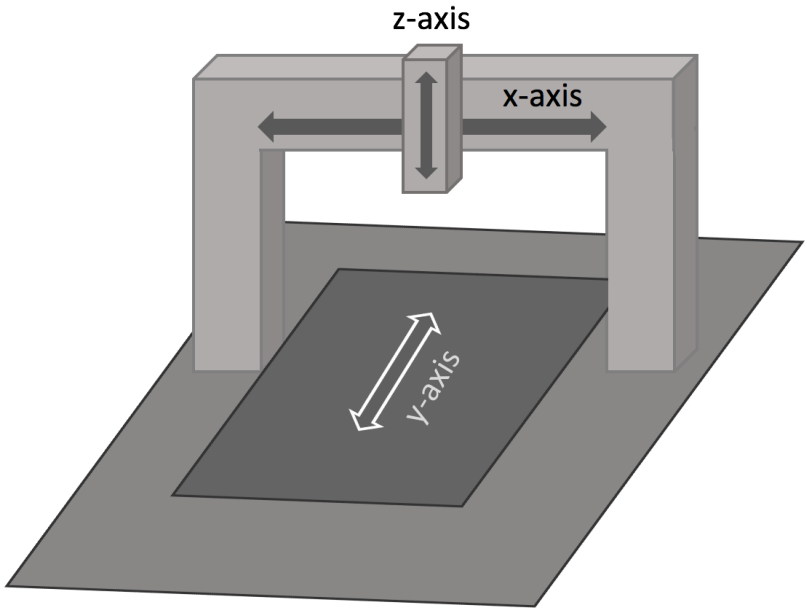


The task of measuring and calibrating a Cartesian linear axis robot is difficult and can be time-consuming and therefore expensive. It is easy to find motivation to develop a measuring system that could be integrated to the robot and possibly fully automated. A significant amount of money and time could be saved by automating the procedure of measuring and calibrating a linear axis machine. The objective of this thesis is to find an answer for the following questions:

1. What geometrical error sources effects X/Y stage motion accuracy?

2. Could a low cost and widely available technology be used as a measurement device?

3. How well does a measurement system built with reduced costs compare with commercial measurement systems?

The current calibration system that is used with the company's test systems requires assembly work before each measurement. This requirement can be costly and thus, automating the calibration procedure is one of the requirements that had more weight when the technologies were selected for this research. Many of the commercial measurement systems available have a bulky construction and cannot be integrated or scaled to a mass production test system. Commercial measurement devices usually always come with a high price tag that makes it impossible to make accuracy measurement integrated accessory to a test system robot. For this reason, building a measurement system with reduced costs has the most weight when searching answer to the questions of this thesis.

## 1.2 Problem approach

As the previous section presented the problem this thesis tries to find a solution, this section introduces methodologies that are used approaching the problem. The first question, what geometrical error sources affect linear axis motion accuracy will be approached by methods of a literature research. Past and more recent studies and other publications such as books are

used for reference for finding reliable information about the theory of linear axis machine motion accuracy and error sources. The literature research will not only concentrate to the geometrical errors but also on other aspects that could have effect to the results. This approach will also look for state-of-the-art solutions of motion accuracy measurement.

The second question about finding a low cost and widely available technology to be used as a measurement device is approached with method of a suitability evaluation. A set of different technologies based on different physical phenomenon will be selected by the company for evaluation. A scoring table will be developed for evaluating technology suitability which includes specification requirements for the technology and which's scores will be weighted in regard of most significance. The technology with highest score will be selected for a proof-of-consept development.

The third question will be approached with validation measurements. A measurement system developed by the company and a commercial measurement device will be used for validating the results of the newly developed measurement system. All measurement systems will be used to measure the same robot and results are compared to draw conclusions.

## 1.3 Thesis outline

This thesis has been divided into Chapters as follows. Chapter 2 introduces the main error sources of a Cartesian linear axis machine and how they contribute to total sum of error. The chapter provides necessary background knowledge of the error sources which are the main interest points. Chapter 3 introduces some basics of calculating measurement uncertainty and how uncertainty sources are categorized in two main groups. Chapter 4 introduces selected technologies for the research study and evaluates their specifications and performance characteristics for building a prototype measurement system. Chapter 5 introduces the developed prototype measurement system and its main functionality from hardware design to machine vision algorithms, data analysis and other software components. The measurement results of the developed prototype measurement system are opened and reviewed. In chapter 6 the measurement results are validated by comparing them to results of commercial measurement system results. Chapter 7 provides conclusions of this thesis work.

# 2 ROBOT POSITIONING AND GEOMETRICAL ERROR SOURCES

This chapter introduces the main error sources that a precision design engineer or a validation engineer faces when designing or measuring accuracy and repeatability of high precision machine such as a milling machine, lathe or a gantry industrial robot. Whether it's about the mentioned high precision machines or any machine with linear axis motion, these inherent and inevitable error sources are always present and not to be neglected.

In precision machine design, the sources of errors are referred as "natural enemies" of the precision engineer. These errors are also referred as "systematic errors" and errors that have no obvious repeatable clear source as "random errors". If one wants to closely look for the root cause for these errors to prevent or minimize them, the task becomes a matter of how much time and money one is willing to spend. When the errors are either measurably fit to the design specification or they are not measurable at all the errors are accepted. [4].

## 2.1 State-of-the-art solutions

This section introduces two commercial state-of-the-art high precision motion accuracy measurement systems which both could be used for measuring linear axis motion accuracy. Both solutions utilize optical measurement method, but they are based on different technologies. Neither one of the systems are designed to be permanently integrated to a measured machine and will always require manual alignment and/or external part installation to the measured machine.

The measurement system in figure 2.1 is Leica AT930 absolute interferometer developed by Hexagon. It utilizes laser interferometry to measure motion accuracy giving it high-speed dynamic measurement capabilities. It is designed for variety of applications not only for linear axis motion accuracy measurement and it uses a 3Dimensional tracking system to track a retroreflector attached to measured system. Leica AT930 can accurately measure motion in a volume for example a 6DoF robot 360-degree workspace up to 160m spherical diameter measurement range. The manufacturer specifies the devices' measurement accuracy to +/- 15 µm + 6$\frac{\mu m}{m}$. Measurement accuracy decreases by 6 µm when measurement distance is increased by one meter [12]. Measurement distance in the subject of this thesis is less than one meter so the given +/- 15 µm can be used when comparing results. The Leica AT930 measurement system is in the price range of about 100k€ which exceeds the scope of this thesis with a huge margin.

***Figure 2.1.*** *Leica AT930 Absolute interferometer[12]*

KGM182 grid encoder in figure 2.2 is developed by Heidenhain which can be used for any x/y stage motion accuracy measurement. The measurement system consists of a measurement head and a waffle-type graduation on a grid plate that is made from titanium which has a low thermal expansion coefficient. The measurement head and grid plate and the waffle-type graduation can be seen in figure 2.2 in more detail. The scanning head is moved over the grid plate during measurement. The scanning head can simultaneously read motion from two perpendicular axes x and y. As the scanning head moves over the plate it produces a sinusoidal 1Vpp output from both axes. Both axes (channels) have a 4 µm signal period. The manufacturer gives the measurement system a +/- 2 µm accuracy grade. The KGM182 grid plate has a 230 mm diameter which limits the measurement range. KGM182 measurement system is in price range of about 5-6k€.[5]

***Figure 2.2.*** *Heidenhain grid scale[5]*

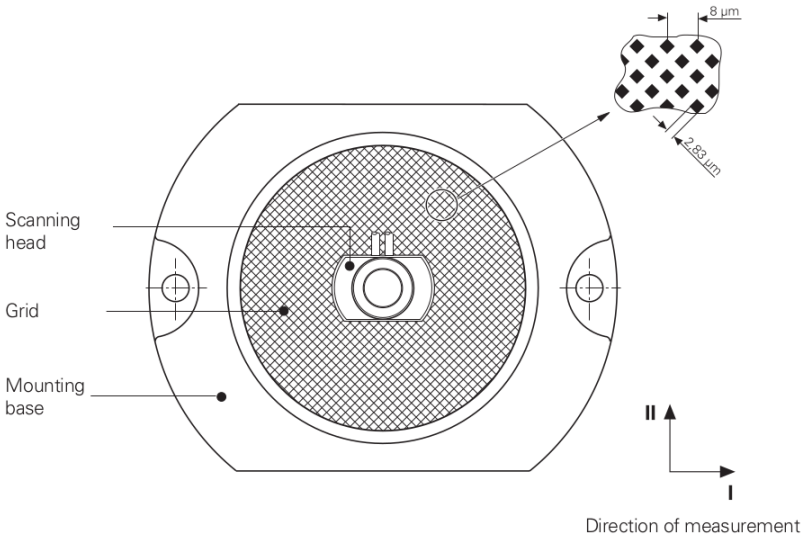

## 2.2 What is accuracy

In the field of robotics, accuracy means the robot's capability to move the center of the end-effector to the commanded or desired position in its coordinate system. In other words, the numerical value of dimensional accuracy represents the degree to which displacements executed by a positioning system match to the desired position which are agreed upon standards of length. Inevitably, all length measurements are tied to the meter, which is defined by the Committee Consultif pour Definition du Meter. The meter is the length of the path travelled by light in vacuum during a time interval of 1/299 792 458 of a second. It follows that the speed of light in vacuum is $c_0 = 299792458m/s$. When describing robot positioning accuracy, a variety of units considerably smaller than a meter are employed. Within the context of this thesis most used unit is the micron ($10^{-6}m$). To give the person reading this a reference for comparison reasons, a human hair is approximately 50-100 µm in diameter. [19]

## 2.3 Resolution and repeatability

### 2.3.1 Resolution

Resolution of positioning system is, simply the finest step of motion still resolvable. It is defined as a single count. This could be the size of a single stepper motor step in open loop controlled system, or the finest increment of motion measurable by the positioning system feedback encoder in a closed loop controlled mode [4].

Consider a linear servo motor whose motion is measured with a linear encoder. The resolution of this particular system is represented by smallest amount of linear motion that can be measured by the linear encoder [7]. For example, if the linear encoder uses magnetic scale for motion sensing and produces 1024 incremental signals for each pole pair of 2 mm in length on the scale, the encoder resolution is then $\frac{2\,\mathrm{mm}}{1024} = 0.001\,95\,\mathrm{mm}$. In this case the smallest positional increment still resolvable is 1.95 µm

### 2.3.2 Repeatability

As the term repeatability suggest, it defines the robots or any other positioning system's ability to repeat motion or measurement within certain bounds. The repeatability of one of these system is the extent to which the repeated positioning to a specific point in the coordinate system vary in position. A system with high repeatability, which repeated moves exhibits a low scatter of measured position when the position is approached each time from the same direction is said to be unidirectionally repeatable. Its counterpart bidirectional repeatability is, naturally, measured when the specified position is approached from two opposite directions. The bidirectional repeatability can be twice the unidirectional repeatability, or even worse, depending on the system composition [4, 15, 18].

As the subject of this thesis is constrained to a two-dimensional coordinate system, repeatability can be visualized like shown in the figure 2.3. If this two-dimensional positioning system is commanded N times to move to the same point in its coordinate system, the repeatability can be measured by the diameter of the smallest circle where all the measured points of the actual achieved positions of each move repetition are enclosed. Also referred to as Spatial Resolution.

***Figure 2.3.*** *a, b, and c: Accuracy vs. Repeatability [4].*

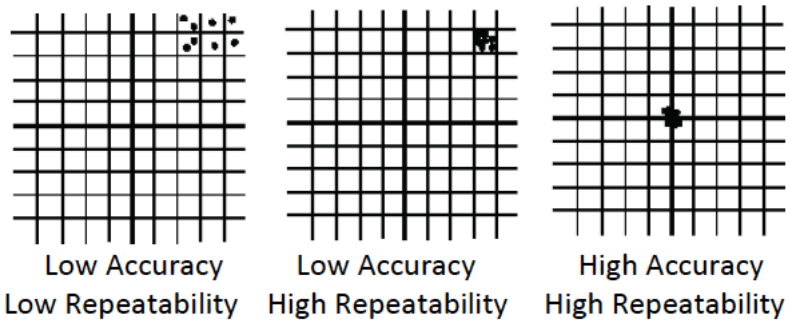


## 2.4 Geometric errors in a three linear axis machine

In terms of geometric errors, these quasi-static errors are always present in a linear axis machine. The errors can be considered representing quality of the machine's original-build and basic design. These inherent inaccuracies are of course, unintentional, which are built-in to the components and part-assemblies used in the actual-build of the machine. They occur during part manufacturing and in the assembly phase of the machine. Geometric errors can potentially be the greatest sources of inaccuracy in the machine. [16] These inaccuracies usually appear as orthogonality, parallelism, translational and rotational errors respect to the three linear axes of motion which all can have a significant impact to the total motion accuracy. Typically, the most unwanted error sources are those which creates an angular error to the robot geometry. Deviation in the robot axis orthogonality or parallelism creates angular errors. [7] A typical three axis Cartesian robot has 21 error components which all contribute to the total sum of positioning error caused by the errors in its geometry. These 21 errors consist of [4]:

- 3 linear positioning errors
- 6 straightness errors
- 9 angular errors
- 3 squareness errors

These errors are listed in the table 2.1.

***Table 2.1.*** *21 geometric causes of systematic error in a three linear axis machine [4]*

| Linear motion | Linear displacement error | Straightness error | Angular error (A=Roll, B=Pitch, C=Yaw) |
|---|---|---|---|
| X-Axis | $E_{xx}$ | $E_{yx}, E_{zx}$ | $E_{Ax}, E_{Bx}, E_{Cx}$ |
| Y-Axis | $E_{yy}$ | $E_{xy}, E_{zy}$ | $E_{Ay}, E_{By}, E_{Cy}$ |
| Z-Axis | $E_{zz}$ | $E_{xz}, E_{yz}$ | $E_{Az}, E_{Bz}, E_{Cz}$ |
| Squareness error | $E_{Sxy}, E_{Sxz}, E_{Syz}$ | | |

The system object to the measurements in this thesis is a Cartesian robot built from three linear translation stages that restricts the application load to a linear three degrees of freedom. From the typical behavior of the robot's linear axis when in use, it is possible to identify six of the error sources relative to the three axes of motion. If the axes were ideal, they would completely restrict the two translation errors and the three rotational errors, thus allowing motion only in the nominal direction of motion. In reality, it is extremely difficult, if not impossible to build an ideal guiding

system. The linear motion guiding system will always bring about the angular deviations and the translation errors. The first three of them are positioning error motions in the point of interest moving a straight-line trajectory, the first of them $E_{XX}$ being along the nominal direction of motion and the other two $E_{YX}$ and $E_{ZX}$ being along two directions orthogonal to this direction. The error motion along the nominal direction of motion is called linear positioning error and the other two error motions orthogonal to this are called straightness error motions [18]. The remaining three angular errors $E_{AX}$, $E_{BX}$ and $E_{CX}$ are the three rotational degrees of freedom which are traditionally referred as roll ($E_{AX}$, rotation around X-axis), pitch ($E_{BX}$, rotation around Y-axis affecting the X-axis position) and yaw ($E_{CX}$, rotation around Z-axis affecting the X-axis position)[4]. These six error motions are visualized in the figure 2.4 and 2.5.

***Figure 2.4.*** *Six degrees of freedom relative to three axes of motion[18].*

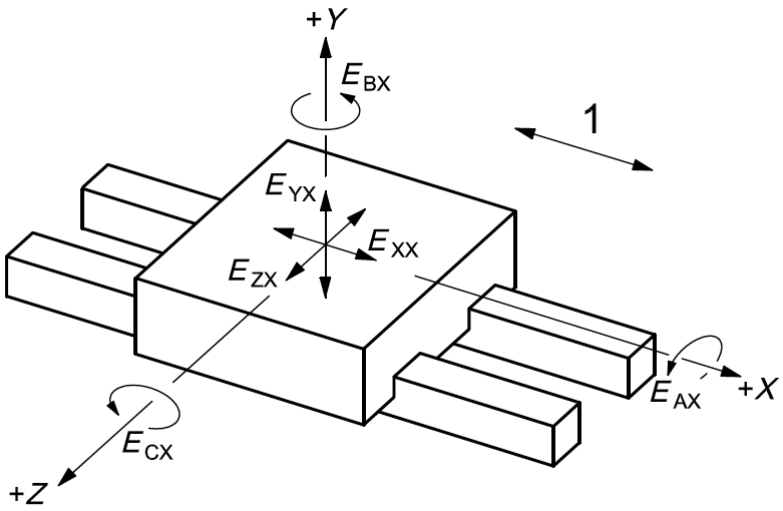


***Figure 2.5.*** *Representation of straightness deviations of X-axis in Y- and Z-axis direction[18].*

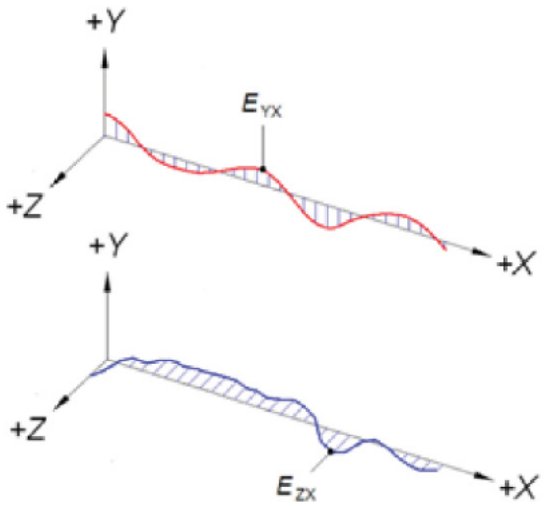

### 2.4.1 Abbé's principle and Cosine error

The robot's geometric angular errors are called Abbé errors. This kind of angular error can be significant error contributor in positioning systems. Abbé error refers to a linear error and it is caused by the combination of angular errors. Typically, this error appears in the ways that define the motion and as an angular offset between the interest point of measurement (a robot axis linear path in this case) and the accuracy determining element [4].

Abbé observed that "*If errors in parallax are to be avoided, the measuring system must be placed co-axially with the axis along which displacement is to be measured on the workpiece*" [4].

Basically, the line of measurement should coincide with the measuring line of the instrument. The simplest examples of instrument designs which violate and obey Abbé are the dial caliper and micrometer, respectively. In the case of the caliper, any distortion of the jaws and their tips (the point at which the measurement is made) will result in an error in the reading of jaw displacement on the scale located at the base of the jaws, the micrometer, by contrast, has the scale for measurement in line with the tips of the jaws and no Abbé error results. [4]

***Figure 2.6.*** *Sine and cosine errors*

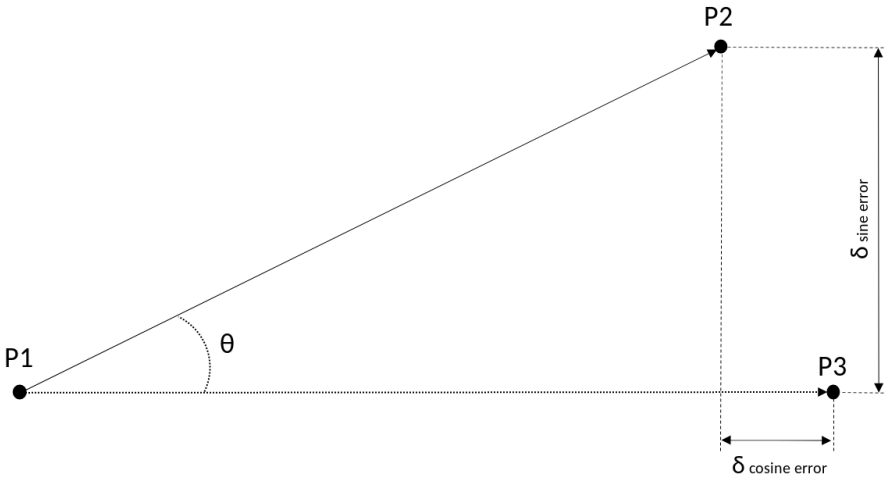


Misalignment between the motion of the point of interest and the accuracy determining element, is the cause of cosine error. This source of error, in most circumstances, has a small effect on the positioning system total sum of errors. Misalignment between the two points must be significant to cause a considerable influence on the total accuracy [4]. For example, let us consider a case where a linear encoder is pitched so that it is inclined to the direction of motion. In the figure 2.6 the point P1 is starting point where the robot is commanded to movo to point P3. Caused by the misalignment, the encoder measures the distance between points P1 and P2. Now the misalignement yields the errors $\delta_{cosineerror}$ and $\delta_{sineerror}$.

# 3 MEASUREMENT UNCERTAINTY

What does "measurement uncertainty" mean? Within this thesis, measurement means effort to characterize a physical quantity describing a robot axis motion performance, using a device capable to detect and measure motion. The term "uncertainty" refers to doubt that exist in the result of these measurements and to a margin of that doubt. These two terms, doubt and margin, both raise a question: "How much there is doubt?" and "What size is the margin?". Finding an answer to both of these questions will provide two numerical values that are required for quantifying quality of the measurement. These two values are represented as the width of the margin and as the level of confidence. The confidence level provides a number that states how sure one is that the actual value is lies within the limits defined by the size of the margin or uncertainty interval. [16]

These two values are obligatory when reporting measurement results describing a physical quantity. The confidence level and width of the margin are the quantitative indication of the quality of the measurement results. Without the values, any measurement result cannot be reliably accessed nor can the results be compared, either among themselves or with any reference values provided by standard or specification. For one to be able to provide reliably comparable measurement results, it is necessary to have a readily implemented and generally accepted procedure for evaluating and expressing measurement uncertainty.

In order to define the uncertainty interval with some level of confidence, statistical measures are be used. The main two mathematical expressions required are the arithmetic mean and the estimated standard deviation. Within this discussion, the arithmetic mean is being denoted by the symbol $\overline{x}$ and standard deviation with the symbol [16].

$$\overline{x} = \frac{1}{N}\sum_{i=1}^{N} x_i \tag{3.1}$$

$$s = \sqrt{\frac{1}{N-1}\sum_{i=1}^{N}(x_i - \overline{x})^2} \tag{3.2}$$

When reporting the result, one way of expressing the level of confidence is to say that "*the true value of displacement is 3.113 $\pm$ 0.012 mm in at 90% of confidence*". This mean that the person who conducted the measurement is 90% confident that the true value lies within the given uncertainty interval. Another way of giving the result of the same measurement would be to say that "*the true value of displacement is 3.113 $\pm$ 0.012 mm in at 10% significance*". This means that there is a 10% chance of a significant event where the true value is not within the given uncertainty interval [13]. Confidence and significance are tied together by:

$$Confidence + Significance = 100\% \tag{3.3}$$

## 3.1 Type A and Type B Elemental uncertainties

Every transducer comes with its own inherent elemental uncertainties. As one of the goals of this thesis is to evaluate pre-selected technologies and find the most suitable one out of them, any elemental uncertainties of those technologies cannot be ignored. Usually the better quality transducer technology will have less uncertainty. The elemental uncertainties are always associated with a particular measurement and not with a test result or calculation, thus they are related to the accuracy of measured quantities. The transducer quality is not the only source of uncertainty. The variability of the measurand that is being measured brings its own uncertainties to the equation. As an example, the thickness of a machined plate shaped part with strict tolerances is measured with laser device. The measurement device will have some certain accuracy characteristics. Also due to size variations in the part the thickness will vary between measurement points. As the laser displacement device is most likely calibrated, its calibration certification will include the total effect of all elemental uncertainties that are produced by the device [13, 16]. Both sources of measurement "error" are elemental uncertainties.

Before the total effect of all uncertainties can be summarized, all sources have to be defined and categorized. These categories are based on the nature of the source of uncertainty which can be thought of as those that are repeatable and those that vary. If the variation of the source of uncertainty can be statistically analyzed, which means that it obeys the law of some statistical distribution such as normal distribution or uniform distribution the source of uncertainty belongs to the category of Type A [13, 16].

***Figure 3.1.*** *Normal distribution[1]*

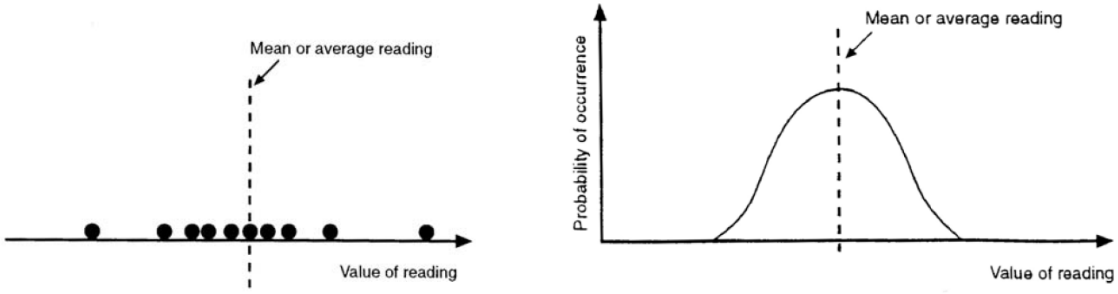


This means that measurement result will vary from time to time or place to place and the quantity of the source can be estimated with the properties of statistical distribution such as the arithmetic mean and standard deviation. To be able to use these properties it allows one to try to predict the range in which the next event is likely to occur but not the actual value of that event. In the category Type B, sources of uncertainty are more repeatable or systematic type. These uncertainties cannot be analyzed with statistical means. This is due to systematic not having any variability[13, 16]. This comes to a conclusion that if the nature source of uncertainty is treated as random and it is analysed with the properties of statistics, the uncertainty belongs to the category Type A. Most of the random uncertainties are Type A uncertainties. These will vary with each measurement taken and can be reduced with a lot of measurements. And any uncertainties that cannot be quantified with statistical analysis are treated as Type B uncertainties. These uncertainties can be estimated with information from certified reference material, calibration certificate, accuracy class of a verified measurement device and from limits deduced through personal experience [1]. Usually most of the systematic or repeatable uncertainties are Type B uncertainties.

***Figure 3.2.*** *Uniform distribution or rectangular distribution [1]*

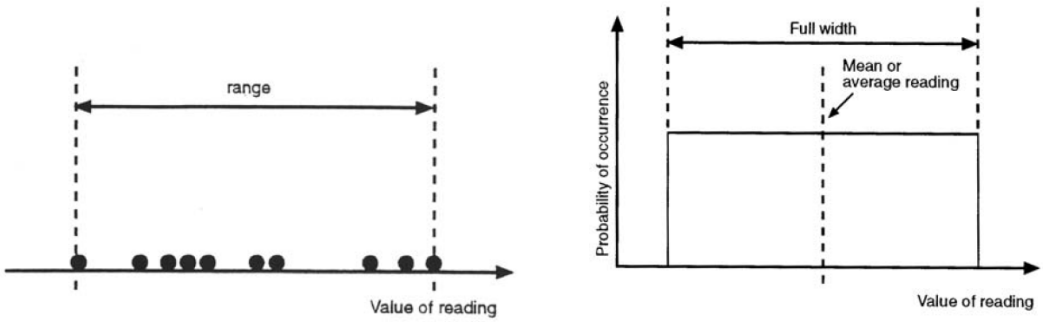


## 3.2 Standard uncertainty

To be able to summarize the total effect of uncertainty, all of the contributing elemental uncertainties should be expressed with the same level of confidence so that they can be combined. This is done with a method of numerically combining the elemental uncertainties which will produce quantity of standard uncertainty of a particular measurement. All of the contributing elemental uncertainties that are being combined, must first be converted into same units. The standard uncertainty quantifies the uncertainty of mean. Standard uncertainty is denoted with the symbol *u* [1, 13].

When calculating standard uncertainty for an elemental uncertainty defined as Type A, a set of readings/measurement have to be taken. For the set of values acquired, the equation 3.1 introduced in section 3 is used for calculating the mean value denoted with $\overline{x}$. Another value required to evaluate Type A standard uncertainty is the standard deviation which is calculated with the equation 3.2. With these values the Type A standard uncertainty can be estimated with the following equation:

$$u = \frac{s}{\sqrt{n}} \tag{3.4}$$

where *n* equals the number of readings/measurements in the set [1, 13].

When calculating the standard uncertainty regarding the Type B elemental uncertainties, it might be possible to estimate only the upper and lower limits of uncertainty due to the information available as listed earlier in this section. Due to this, one may have to assume that the value of a reading or a measurement is as likely to occur anywhere in between the upper and lower limit. This is called a uniform distribution or a rectangular distribution3.2.

In the case of Type B elemental uncertainty which obeys the rectangular distribution, the standard uncertainty can be found using the following equation:

$$u = \frac{a}{\sqrt{3}} \tag{3.5}$$

where *a* is the half-range or half-width of the upper and lower limits of the rectangular distribution.

## 3.3 Combined standard uncertainty and Expanded uncertainty

Prior to the calculation of expanded uncertainty that is the goal of uncertainty analysis, both of the elemental uncertainty categories need to be combined. This can be done with the method of summation in quadrature or the root sum of squares (RSS). This step of the process will produce the combined standard uncertainty $u_C$ [1, 13]. Using the following method to calculate the combined standard uncertainty is correct only if all the input uncertainties are uncorrelated. This means that all of the contributors are independent of each other and a change in one uncertainty does effect any other source of uncertainty. Within this thesis all elemental uncertainties are assumed to be uncorrelated.

Type A combined standard uncertainty:

$$u_A = \{\sum_i u_{A,i}^2\}^{1/2} \tag{3.6}$$

Type B combined standard uncertainty can be found with the same equation using the Type B standard uncertainty:

$$u_B = \{\sum_i u_{B,i}^2\}^{1/2} \tag{3.7}$$

Standard uncertainty of a particular measurement:

$$u_C = \sqrt{u_A^2 + u_B^2} \tag{3.8}$$

As discussed earlier in this chapter the uncertainty of a measurement includes the uncertainty interval and the confidence level. With the combined standard uncertainty, it is now possible to find the expanded uncertainty of a measurement which includes both of the mentioned parameters. To find the final result of uncertainty of the measurement the calculated uncertainty interval i.e combined standard uncertainty need to multiply with a parameter called *k*-factor or coverage factor ('*k*'). In the table 3.3 coverage factor values are listed for different levels of confidence. Often the confidence level of 95% is used which correlates to a coverage factor('*k*') of 2. As seen from the table, the *k*-factor of 2 is an approximate of 95% confidence level and the actual theoretical confidence level corresponding to the *k*-factor of 2 is 95.45%.

***Figure 3.3.*** *Coverage factors for different levels of confidence [13]*

| Confidence (%) | Significance (%) | Theoretical *k*-factor | Approximate *k*-factor |
|---|---|---|---|
| 68.27 | 31.72 | 1.000 | |
| 70 | 30 | 1.036 | 1 |
| 80 | 20 | 1.282 | 1.3 |
| 90 | 10 | 1.645 | 1.6 |
| 95 | 5 | 1.960 | 2 |
| 95.45 | 4.55 | 2.000 | |
| 98 | 2 | 2.326 | |
| 99 | 1 | 2.576 | 3[a] |

Expanded standard uncertainty can be found with the following equation:

$$U = k * u_C \tag{3.9}$$

where $k$ is the $k$-factor of the used confidence level. This equation produces the final result of expanded uncertainty in measurement.

## 3.4 Metrological traceability

Metrological traceability is defined by the JCGM as a property of a measurement result that can be related to a reference through a documented unbroken chain of calibrations, each of them contributing to the measurement uncertainty [10]. As the subject of this thesis is about position measurement, the related reference used is the international standard of length which is the primary standard utilized to calibrate reference standards when measuring distance [16]. The measurement traceability is an important aspect in position sensor development and validation. The measurement error of the designed position sensor must be compared and evaluated with respect to the true position obtained from a reference sensor. The obtained true value will also include measurement error from the reference sensor calibration errors. To quantify the measurement error tolerances for the newly developed position sensor, tolerances of used reference sensors need to be known. This means that the unbroken chain of calibrations is known from the international standard of meter to the reference sensor. As the chain of calibrations is valid, the measurements produced with the new position measurement sensor can be added to be the last link of the chain of calibrations. Now the measurement results can be directly related to the reference and it will have the property of metrological traceability. Each step in the chain of calibrations will add uncertainty to the measurement result. This is why it is reasonable to try to link the instrument to the reference standard through the least number of intervening measurement instruments [6].

# 4 EVALUATION OF POSITION MEASUREMENT TECHNOLOGIES

In this Chapter the pre-selected position measurement technologies are shortly presented based on their basic detecting principle. Each presented technology will be then evaluated with a set of specification criteria and constrains listed in the next section. The evaluation is conducted to measure suitability of each technology to be used in the position measurement system. The technologies are capable of measuring object displacement, direction of motion, speed and acceleration. The following sections gives a general introduction to the technologies and used methods of transforming physical measurands to digital data.

Many position measurement applications have been developed using a variety of different sensor technologies based on different physical measurands. This thesis categorizes the technologies to two groups optical sensors and non-optical sensors and focuses only to evaluate the optical sensing technologies. The main function of a sensor in high precision positioning system is to measure distance or displacement of the point of interest respect to a reference point. Optical position measurement is non-contact measurement and thus has advantage to other sensor types which can add error to the measurement due to mechanical contact. The non-contact measurement is why other than optical sensing technologies are not included to the evaluation.

The technologies will be scored based on the characteristics listed in the table 4.1. Each item in the table has individual weight to the final score.

***Table 4.1.*** *Technology evaluation criteria*

1. Cost: Price estimate of the required components. [-2;2]
2. Automation: Requires human interaction. [0;1]
3. Integrability: Rate of integrability to robot solution. [-1;1]
4. Accuracy: Estimation of achievable precision. [-1;1]
5. Area: Size of the measurable area. Referenced to 400x400mm area. [0;1]
6. Error sources: Number of measurable error sources. [-1;1]
7. Standardization: Measurement traceability to the definition of meter. [0;1]
8. Point of measurement: Measures tool center point position. [0;1]
9. Repeatability: Estimation of achievable repeatability. [-1;1]
10. Resolution: Estimation of the smallest resolvable increment the system is capable of measuring. [-1;1]

## 4.1 Optical interferometry

Optical interferometry is widely used in calibration of machines with high precision positioning requirements. It utilizes the phenomenon of wave interference to measure displacement which in this case is produced by using laser light waves. This phenomenon of interference is produced when two beams of light superpose. This creates an interference fringe pattern which is used for calculating displacement. A laser interferometer based on the Michelson's principle was selected for the evaluation.

Michelson's interferometer uses a single coherent and stable light source which is divided into two beams with a polarizing beams plitter. Both beams are transmitted to retroreflectors that reflects the beams back to the beam splitter. As the beams hit the beam splitter they are combined and transmitted to a detector element that analyses the fringe pattern. One of the retroreflectors is fixed on its place and the another moves with the measured object [9].

***Figure 4.1.*** *Michelson's interferometer [9]*

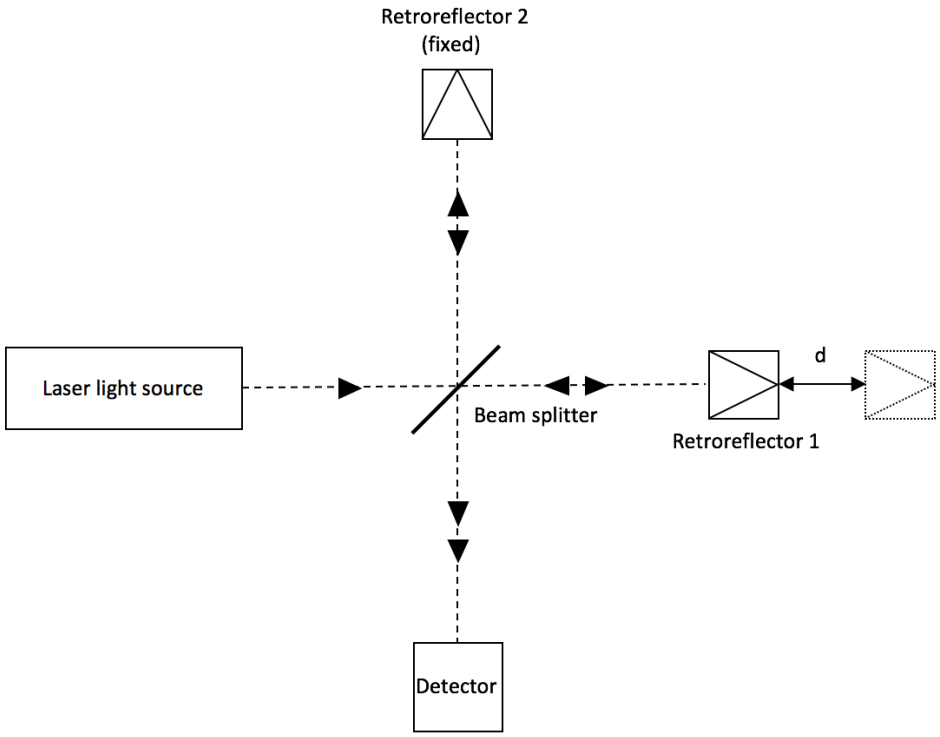


This creates a difference in the beam paths and in their phase. If the beams are in phase when they reach the detector, they interfere constructively, resulting a higher amplitude and a brighter fringe pattern. Destructive interference occurs when the two beams are out of phase and cancel each other, resulting lower amplitude and dark fringe pattern. As the measured object moves, it causes a change in the relative phase of the beams. The detector detects change in the intensity of the light reaching the detector. The intensity changes in cycles caused by the constructive and destructive interference. As the wavelength of visible light is very short, small changes in displacement causes changes in the beam phase [9].

$$d = \frac{\lambda N}{2} \tag{4.1}$$

where $d$ is the displacement moved by the target object, $\lambda$ is the laser light wavelength and $N$ is the fringe counter value. More detailed information and examples can be found from literature such as in [9].

***Table 4.2.*** *Optical interferometry score summary*

| Item | Argument | Points |
|---|---|---|
| 1. | High HW costs >10k€ | -2 |
| 2. | Not possible to automate | -1 |
| 3. | Not integrable | -1 |
| 4. | Very high accuracy | 1 |
| 5. | Measurable area > reference | 1 |
| 6. | All | 1 |
| 7. | Traceable | 1 |
| 8. | Yes | 1 |
| 9. | Highly repeatable | 1 |
| 10. | < 1 µm | 1 |
| Total | | 4 |

## 4.2 Optical triangulation

Laser triangulation sensors use reflected light from the target surface to measure distance to the target. The operating principle of laser triangulation displacement sensor is based on a CMOS/CCD or PSD detector, a solid-state laser light source and focusing optics. The sensor projects a laser beam to the target under measurement and distance is calculated from the part of the beam which is reflected via the focusing optics onto a detector. When the distance between the sensor and target changes, the reflected laser beam proportionally moves on the detector surface. [2]

The laser triangulation devices that employ CMOS sensor as the main light detecting element, detect the amount of light in each individual pixel on sensor surface. The location of the peak value of the spot beam reflected from the target onto the CMOS sensor is converted into distance. The peak value is found by reading out all of the sensor pixel voltage values and beam center point is at the pixel with the highest voltage value [17].

***Table 4.3.*** *Optical triangulation score summary*

| Item | Argument | Points |
|---|---|---|
| 1. | Low HW costs <0.5k€ | 1 |
| 2. | Possible to automate | 1 |
| 3. | Integrable | 1 |
| 4. | Low accuracy | -2 |
| 5. | Measurable area < reference | -1 |
| 6. | Only errors that coincide | 0 |
| 7. | Traceable | 1 |
| 8. | Yes | 1 |
| 9. | Repeatable <= 50mm range | 0 |
| 10. | < 1.5 µm <= 50mm range | 0 |
| Total | | 3 |

***Figure 4.2.*** *Laser triangulation principle [2]*

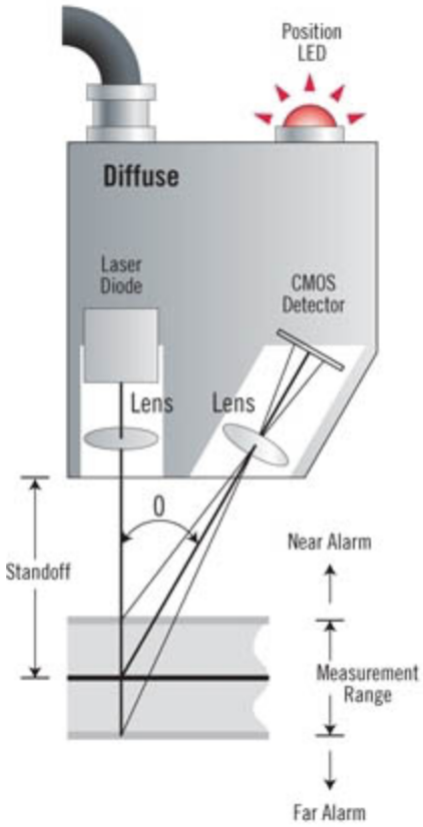


## 4.3 Vision based measurement

Due to reduced cost and component size, Machine Vision has become easier to develop and to apply in Vision Based Measurement systems. The most common tasks where a Vision Based Measurement system are employed are monitoring and measuring a physical phenomenon as a generic instrument. But if machine vision is to be applied in Instrumentation and Measurement as a system's overall accuracy defining element in an industrial environment, further studies and investigations are required. [14]

Vision based measurement can be divided into five stages, acquisition, preprocessing, image analysis and measurement. Additionally, in thesis there would also be 6th stage which is camera spatial calibration due to the nature of the measurement as it requires accurate transition between the image coordinates to real world units. Acquisition stage includes hardware as a visual sensor. Preprocessing stage is for improving the image quality by removing blur, noise, or glare if necessary. Preprocessing can be decreased with enhanced imaging environment by blocking ambient light or other light sources effecting the image. Image analysis includes the case specific imaging operations such as Object tracking, contour detection, pattern recognition, measurand identification and other imaging algorithms. Camera spatial calibration could be a substage of measurement stage where the physical size of visual sensor pixel size is converted to real world units by capturing an image from a known object and calculating the ratio of sensor pixel size and the known object size. In measurement stage after calibration measurements can be done for the identified measurand which could be position, area, volume or other.

***Table 4.4.*** *Vision based measurement score summary*

| Item | Argument | Points |
|---|---|---|
| 1. | Low HW costs <1k€ | 1 |
| 2. | Possible to automate | 1 |
| 3. | Integrable | 1 |
| 4. | sufficient accuracy | 2 |
| 5. | No limit | 1 |
| 6. | 2D geometric + positioning sys | 0 |
| 7. | Traceable | 1 |
| 8. | Yes | 1 |
| 9. | Repeatable | 1 |
| 10. | 5 µm | 0 |
| Total | | 9 |

## 4.4 Optical mouse

The optical image-based computer mice available on today's market have been developed to obtain very high-resolution images and detect motion with high sampling speeds. These features raised the idea of using a high-end optical mouse as a motion detecting element of the position measurement system. Both VCSEL and LED based optical mice have been proven to be used as a displacement or as an odometry sensor. CITE. Both of the technologies have the same working principle which is based on optical sensor including three main parts: light source, lens and image capturing device. The light source emits light through a lens onto the surface under the sensor. Light is reflected back from the surface and lights passes through another lens into to imaging sensor.

***Figure 4.3.*** *Working principle of optical mouse*

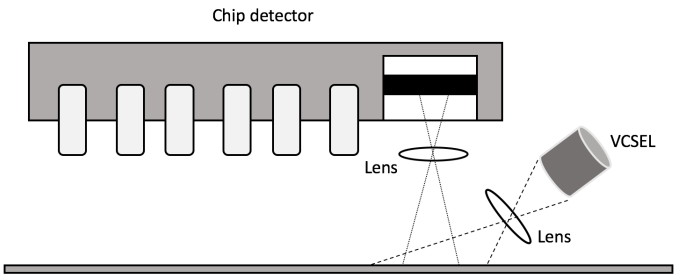


A high-performance optical mouse sensor ADNS-6010 from Avago Technologies was selected for comparison. The ADNS-6010 has a high resolution cpi value which makes it more suitable form displacement measurement than other sensors with different configurations. This particular sensor has 2000cpi resolution. To determine the minimum resolvable step size in millimeters the cpi is converted with the equation 4.2.

2000 cpi (counts pert inch) is converted to mm $\frac{mm/in}{countsperinch} = mm/inch$

$$\frac{25.4mm}{2000cpi} = 0.0127mm \tag{4.2}$$

***Table 4.5.*** *Optical mouse score summary*

| Item | Argument | Points |
|---|---|---|
| 1. | Low HW costs <0.5k€ | 1 |
| 2. | Possible to automate | 1 |
| 3. | Integrable | 1 |
| 4. | not sufficient accuracy | -2 |
| 5. | No limit | 1 |
| 6. | 2D geometric + positioning sys | 0 |
| 7. | Traceable | 1 |
| 8. | Yes | 1 |
| 9. | Repeatable | 1 |
| 10. | 15 µm | 0 |
| Total | | 5 |

## 4.5 Motivation for camera based measurement

The vision-based technology was chosen for the measurement system development and validation phase of this thesis. This section presents the motivation for selecting vision technology with more detail in addition to the high scores from the evaluation - why this technology approach was chosen. The decisive factor was the available equipment including a variety of suitable hardware and algorithms for machine vision applications.

**Cost: Price estimate of the required components:** A camera and lens combination was available for this thesis work without any additional purchase costs. The vision tool combination if purchased would be in below 1k€ price range which is in reasonable limits. A majority of the test systems that this measurement system could be integrated to already includes a camera for other purposes which could be also used for motion accuracy measurement. This makes choosing a camera easier and appealing.

**Automation: Requires human interaction:** The measurement system can be developed to be fully automated utilizing a machine vision-based technology. Calibrating the measurement system would be a part of the test system bring-up and after the system is calibrated, it no longer requires any human interaction and could be operated remotely. The camera holds its calibration if it doesn't get any external interference that could change the lens focus. Measurement target can also be integrated onto the robot's construction which requires no additional part installation to carry out a measurement.

**Integrability: Rate of integrability to robot solution:** As majority of the test system robots include a camera nearly at the most optimal location for measuring motion accuracy the measurement system gets high scores for integrability. A camera installed close to the tool tip can have a large variety of applications. It motivates to desing a construction that a camera and a measurement target integrates to it easily. All of the required parts of a vision-based measurement system can be integrated to robot. A camera does not need extensive cabling and effective cable management is relatively easy to design. Industrial camera that will be used for the measurement system has a small casing and the lens also do not require much space.

**Accuracy: Estimation of achievable precision:** Vision based measurement systems are used in many applications in a variety of technical fields and measurement accuracy is defined by selecting suitable camera sensor size and a lens with suitable focal length and viewing angle. If a pixel size on the camera sensor is around 2 µm $\times$ 2 µm it gives a range of achievable accuracy.

**Area: Size of the measurable area:** In this case the camera will be mounted on the robot's z-axis close to the most interesting position at the tool tip. This way the camera can reach the same area

as the robot's tool can reach covering maximum area of the robots working area. This also enable measuring diagonal or any other type of motion accuracy. As the reference area for scoring was 400x400mm, camera get max points as it can measure the whole area.

**Error sources: Number of measurable error sources:** A camera with a measurement target is able to measure linear displacement error, x/y stage straightness error and angular yaw error of the axis perpendicular to the measured axis. From the table 2.1 measurable errors are linear displacement errors Exx, Eyy, straightness errors Exy, Eyx, angular yaw errors Ecy, Ecx and squareness errors Esxy and Esyx. Total of 8 error sources and the total x and y directional sum of all error sources.

**Standardization: Measurement traceability to the definition of meter:** Traceable measurement results can be achieved by using a calibrated measurement target. This could be for example a machined circle grid or any other pattern of shapes that can be measured with a coordinate measurement machine (CMM). A calibrated CMM has calibration documentation that give it a solid trace to the standard meter and any object measured with the CMM inherits the same trace to the standard meter. The camera spatial calibration could be done with the CMM measured machined circle grid and that way inherit the CMM's traceability.

**Point of measurement: Measures tool center point position:** A camera does not measure the tool tip center point directly but it is very close to the optimal measurement location at the tool tip center point. Offset of the camera optical axis and the tool tip center point can be calculated accurately and then calibrated. The following chapter give a more detailed view for the camera mounting location.

**Repeatability: Estimation of achievable repeatability:** Highly repeatable. Estimate of less than $\pm$ 1 µm. After the camera + lens combination is calibrated which produces constant coefficients for image undistortion, each captured image is undistorted with the same coefficients.

**Resolution: Estimation of the smallest resolvable increment the system is capable of measuring:** High resolution values are achievable by selecting large CMOS sensor size and lens with longer focus length increasing the ppmm (pixels per millimeter) value. Resolution estimation is based on the same conclusions as the earlier accuracy estimation.

# 5 MEASUREMENT SYSTEM DESIGN

This chapter describes designs and functionalities of subsystems which were implemented for building the prototype measurement system. A major part of the prototype is based on software algorithms which are developed with Python programming language. The prototype measurement system can be divided into three subsystems from which two of them are algorithms and one includes all hardware components. These three subsystems are:

- Camera and optics
- Camera calibration
- Imaging algorithms

The following sections and subsections introduce the construction of each subsystem and some basic concepts and working principles of their individual tasks and contribution to the complete measurement system. The mentioned measurement system will be referred as *SUD* from this point onwards, which is short from *System Under Development*. In addition, the SUD includes a calibration and measurement target component which is not a subs system like other three, but it is required in the two software-based subsystems. This component is introduced in the section 5.2

## 5.1 Hardware setup

The figure 5.1 below illustrates a Cartesian robot construction. As seen from the figure the camera is mounted to the vertically moving z-axis. Mounting the camera to the z-axis it is very close to the robots tool center point which is the most interesting location for motion accuracy measurement. Mounting the camera to the z-axis enables changing camera field of view if necessary as the camera can be moved closer to or farther away from measurement target below. Measurement system resolution increases if the camera is closer to the target but it could be beneficial to capture images of a larger area by raising the z-axis and camera higher relative to the measurement target.

***Figure 5.1.*** *Robot axis and camera to target orientation*

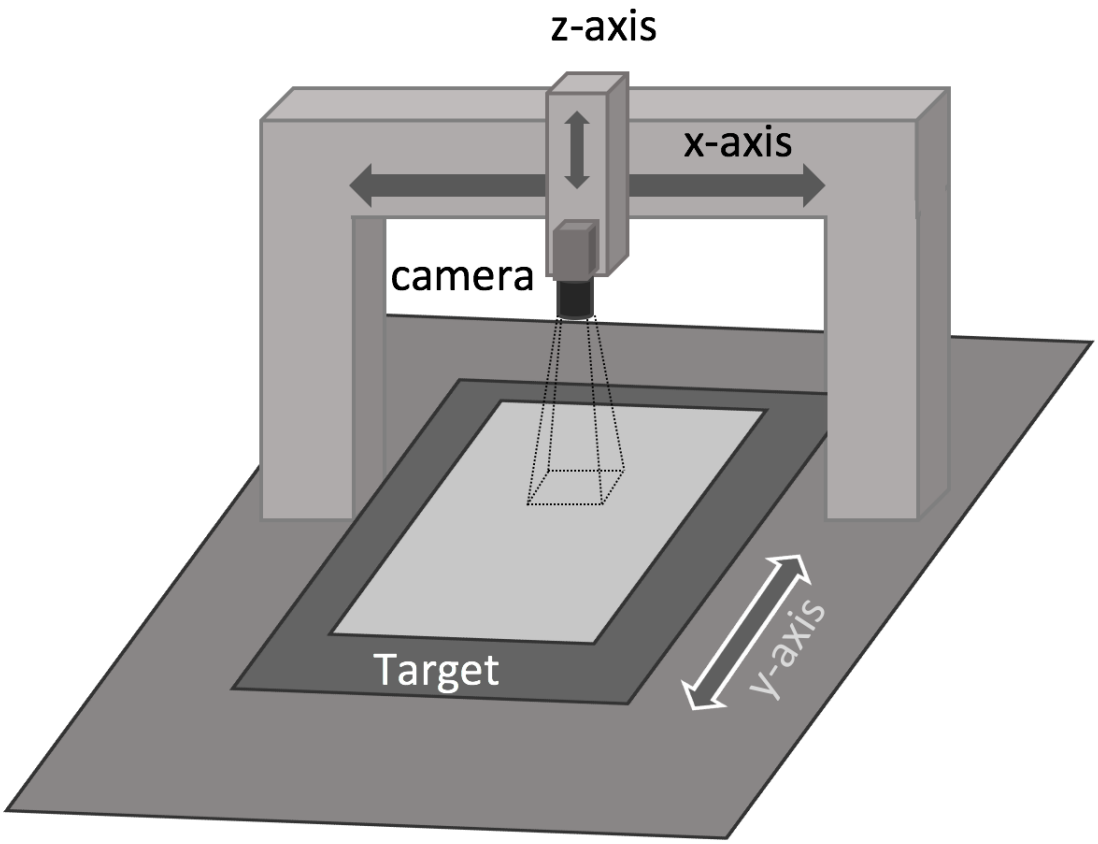


Decision to choose Basler acA2500-14gm camera for development was based on the sensor characteristics, low cost, availability and also to easy integration due to available mechanical interface on the robot's z-axis mechanics. By using this particular camera, no additional mechanical bracket or other holders were necessary to design and manufacture. Also, a python software interface was available for Basler which made it quick and easy to add it to software development. The camera has a small pixel size which is required to get higher measurement resolution. Sensor size is not largest available but sufficient for proof of concept development. Basler acA2500-14gm and Edmund optics lens has the following characteristics:

- **acA2500-14gm**
  - CMOS 5.7 x 4.3mm sensor
  - 2592 x 1944 px resolution
  - 2.2 x 2.2 µm pixel size

- **Edmund optics 8mm**
  - 8mm focal length
  - f/1.8 - f/11
  - 39.24deg Field of View

## 5.2 Measurement target

One of the fundamental ideas in building a low cost measurement system is to use a non-accurate measurement target. In many commercial linear or grid encoders, the measurement requires accurately manufactured linear grating scale or a grid grating plate as the measurement target. For example, some linear grating scales can have a grating with 1µm spacing with low tolerances. The precision required to manufacture these components, ramps up the costs.

One considered design of accurate target to utilize in the SUD was a "similar" grating plate but with much larger spacing. The grating could have been manufactured from steel plate including a set of holes or datum pins that would make the grating/grid with spacing closer to mm or tens of mm rather than in the µm level. The target could have been manufactured with cost efficient tolerances but it would have required calibrating itself. To make the target accurate, it would have required to be measured with a CMM to produce a calibration certificate that includes accurate measurement of distance between each of the grating/grid features. Measuring and creating a calibration certificate for each manufactured target would have raised the SUD costs. For these reason, the SUD is designed to use a non-accurate measurement target.

As discussed in the previous paragraphs, the measurement target must be non-accurate to avoid excessive costs. This led to decision to use a circle grid pattern shown in figure 5.2 which can be displayed on a tablet touch screen. By using a tablet screen, it is quick and easy to generate various images with different circle sizes and grid patterns for testing and developing measurement algorithms which would not be possible with machined targets.

Tablet device used in the measurement has the following screen specifications:

- 12.9 inch diagonal length
- 4:3 aspect ratio
- 2048 x 2732 resolution

Generating the measurement target is done in two phases using python scripts. In the first phase, a script generates multiple images with one circle and resizes them to make the circle diameter exactly to given number of pixels. Knowing the diameter length is required in the second phase. In the second phase, all of the images with on circle are merged into a single image with a specified grid pattern size.

The tablet device specification provides values for aspect ratio, diagonal length and resolution. With these values the screens pixels size can be calculated. The screen has a 12.9 inch diagonal length which is 327.66 converted to millimeters. Using this value and the aspect ratio, the screen width and height can be calculated with the equations in 5.1 and 5.2.

$$\begin{aligned} screenwidth &= \sqrt{\frac{diagonal^2 * aspectratiowidth^2}{aspectratiowidth^2 + aspectratioheight^2}} \\ &= \sqrt{\frac{327.66^2\,\mathrm{mm} * 3^2}{3^2 + 4^2}} = 196.596\,\mathrm{mm} \end{aligned} \tag{5.1}$$

$$\begin{aligned} screenheight &= \sqrt{diagonal^2 - screenwidth^2} \\ &= \sqrt{327.66^2\,\mathrm{mm} - 196.596^2\,\mathrm{mm}} = 262.128\,\mathrm{mm} \end{aligned} \tag{5.2}$$

Dividing these values with the corresponding screen resolution values the pixel size is obtained.

***Figure 5.2.*** *Measurement target circle pattern*

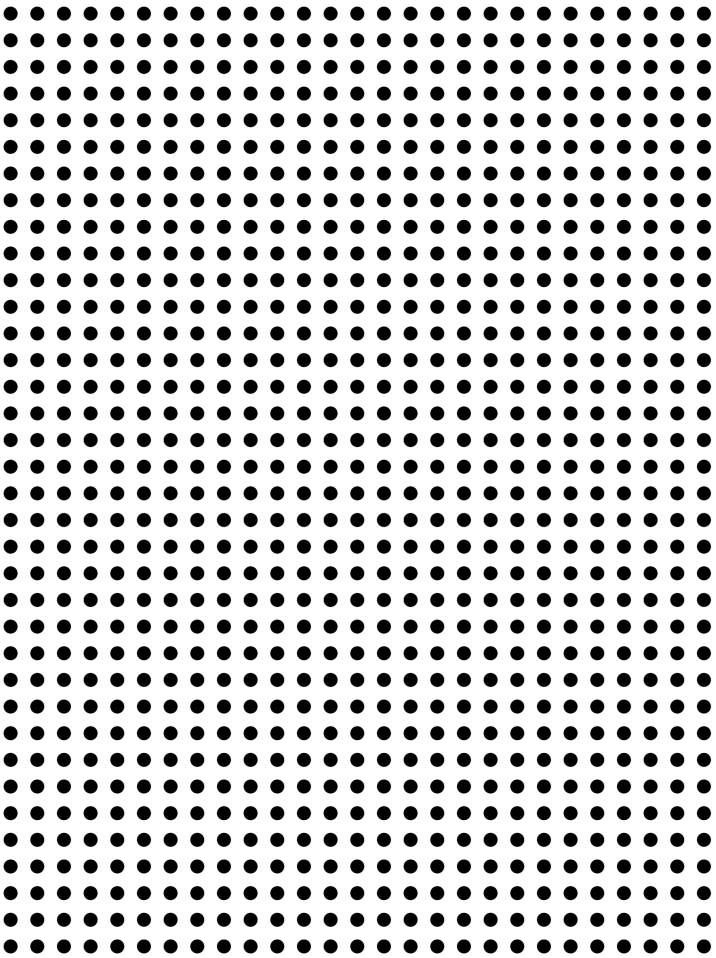

$$pixelwidth = \frac{196.596\,\mathrm{mm}}{2048px} = 0.09599 \approx 0.096\frac{mm}{px}$$

$$pixelheight = \frac{262.128\,\mathrm{mm}}{2732px} = 0.09594 \approx 0.096\frac{mm}{px}$$

screen pixel size is $96x96\,\mu\mathrm{m}$

## 5.3 Software components

This section introduces software components in figure 5.3 that were developed and/or integrated to the measurement system. The systems' software implementation is divided into four main components. Each component has its own task which produces an output for a component next in the execution sequence. Functionality on each component is described in more detail later in this chapter. The four main components are as follows:

**Robot control and Image acquisition:** As the name suggests, this component has two main tasks. This component controls moving the robot axis from one measurement position to another. In each measurement position the robot motion controlling task signals the camera to capture an image of the measurement target. The robot controlling task is given a starting point coordinate and the length it needs to move. For example, when measuring y-axis direction, a starting position

could be (x=100, y=0) and the measurement length could be 100mm. A sequence of positions from (x=100, y=0) to (x=100, y=100) with a 1mm step length is interpolated from these attributes. This sequence will then move the robot with one-millimeter steps from the starting position to the end position and stops after each step to signal the camera to capture an image. Each image is named with the robot x/y position where the image was captured. A string of path to the images is outputted to next component.

**Calibration:** This component handles undistorting the acquired images. It is given a path to the directory where the raw images are stored. Each image is opened and undistorted by using coefficients acquired from the camera calibration procedure and saved to a new directory. The path of this new directory is outputted to the next component.

**Circle detection:** Given a path to the newly undistorted images, this circle detection component goes through all of the images and searches for a circle shape with a given diameter parameter. If the algorithm finds a circle patter that matches the given diameter, it finds the circle center position in the image pixel coordinates. The algorithm searches the whole image for circle patterns and saves the location of all found circles into a text file. At the end of the algorithm's execution, it outputs a path to the file that contains locations of all found circles in all of the images.

**Pattern tracking and Motion analysis:** From the circle center point locations the pattern tracking module searches for a NxM circle grid pattern. From each found circle grid the module calculates the NxM pattern mass center point. The circle grid pattern is tracked from one image to another as long as it is visible. The tracking module passes all circle grid mass center points to the motion analysis module which then calculates distance between each consecutive grid center points. Motion error can be calculated from the measured and commanded motion. These calculated values are then passed to the last module that creates result plots.

***Figure 5.3.*** *Software components*

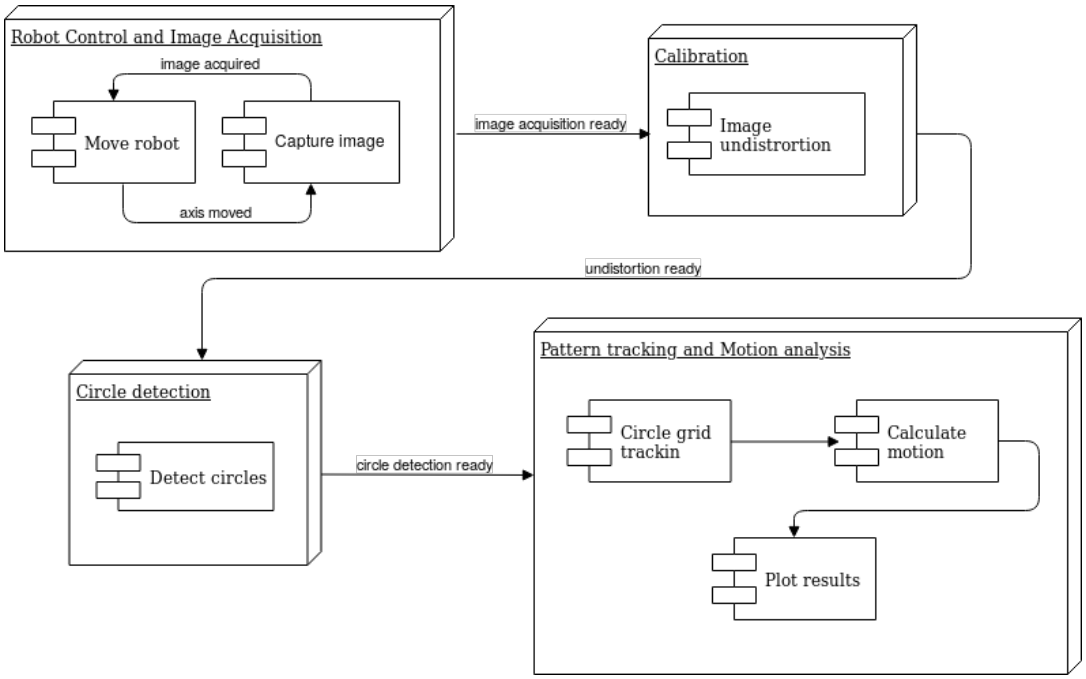


## 5.4 Camera radial distortion calibration

This section introduces some of the basics of camera calibration, that have an important role in the measurement uncertainty and the resulting achievable measurement accuracy. The scope of

this thesis work does not cover any development of camera calibration algorithms nor performance comparison of available solutions, thus this section will not include any algorithm performance studies, which would otherwise be preferable. The utilized camera calibration procedure is protected by the company's IPR. For this reason, the following subsections won't have detailed information about the implementation of the algorithms and will only go through the basics and show example images from the measurement target to give the reader some standpoint of camera calibration and image undistortion.

OpenCV-Python library provides functionality for calculating required parameters for distortion calibration. Its camera calibration module is designed to remove radial distortion from images, which can make straight lines appear to be curved. The image 5.4a shown below is captured from the measurement target and is not undistorted. The rectangle drawn onto the image is aligned with center circle in the first and last column/row. The radial distortion can be clearly seen from the image as the circles in the corners are not overlapping with the rectangle edges. After running the same image through the undistortion algorithm, the effect can be seen in the figure 5.4b, where the radial distortion has been corrected.

***Figure 5.4.*** *Image undistortion*

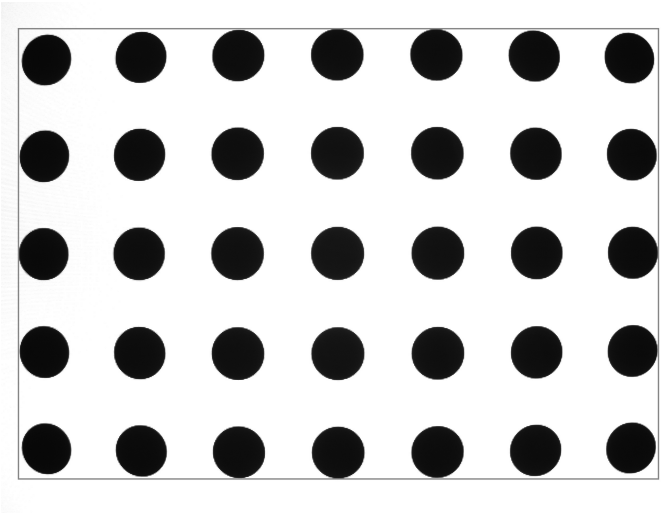

***(a)*** Non calibrated

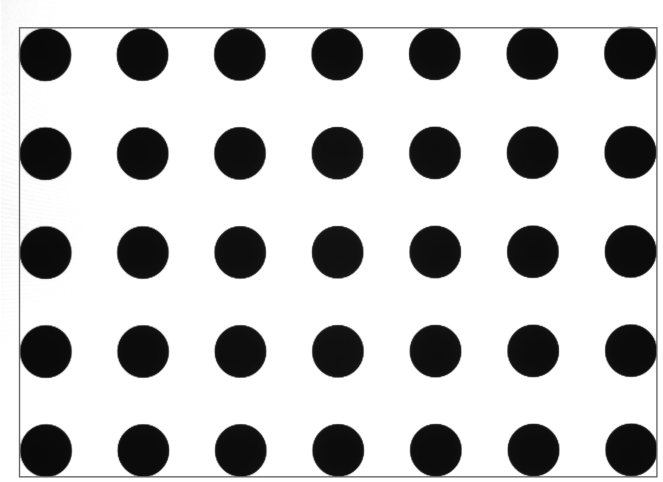

***(b)*** Calibrated

## 5.5 Camera spatial calibration

The abbreviation PPMM stands for *Pixels Per Millimeter*, which is a numerical coefficient used for translating the pixel in an image to actual real-world units of length. The *PPMM* value has a significant impact to the SUD measurement uncertainty and accuracy performance.

The *PPMM* value is calculated within the same algorithm which calculates the camera matrix coefficient. The algorithm uses the freshly undistorted image(s) to find the value in question. The algorithm takes the distance of two circle center points in millimeters as an argument and uses that value to calculate *PPMM*.

$$PPMM = \frac{circledistanceinpixels}{circledistanceinmm} \tag{5.3}$$

For example, a circle center point distance of 335 pixels and 6.234 mm would give a *PPMM* value of 53,737 pixels per millimeter.

The camera ppmm was calculated from multiple images captured from multiple locations covering almost the entire area of the measurement target. A total of 144 images were captured for calculating ppmm and to estimate deviation. These images was captured over three areas shown in figure 5.5.

***Figure 5.5.*** *ppmm image acquisition*

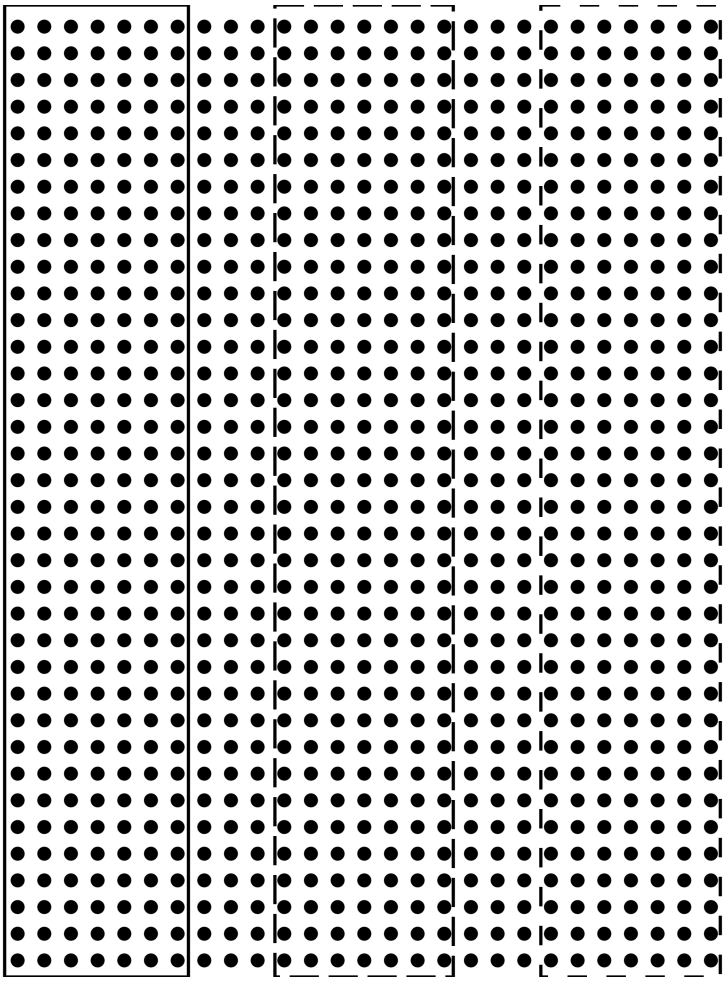

Using the calculated measurement image pixel size camera FOV (*Field of View*) can be calculated by multiplying it with the camera resolution values as shown below.

$$FOV_{width} = 0.0179\,\mathrm{mm} * 2592px = 46.576\,\mathrm{mm}$$

$$FOV_{height} = 0.0179\,\mathrm{mm} * 1944px = 34.932\,\mathrm{mm}$$

***Figure 5.6.*** *Field of View size*

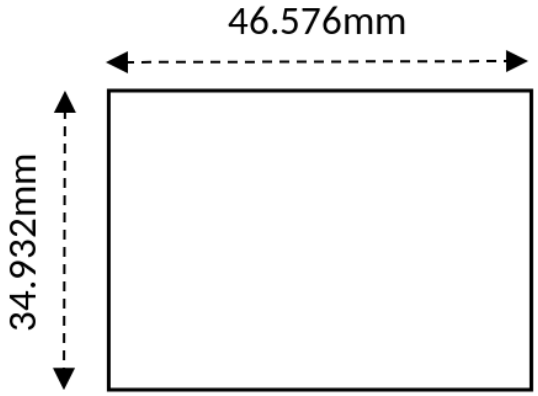


## 5.6 Image acquisition and data extraction

The subjects introduced in the previous sections are prerequisites for the actual measurement algorithm. This section describes the methods of acquiring measurement images, extracting data from the images and how the data is analyzed to determine distance moved between images.

First stage of the measurement sequence is capturing images from the target as it is moved with the measurement axis or the camera is moved above the target depending on which axis is being measured. In the figure 5.7 the two rectangles represents the area covered by camera FOV as it moves respect to the target. The axis is moved with configurable length incremental steps from a starting point in robot coordinates for a given number of steps. For these measurements the incremental step length was set to one millimeter. After each moved step the camera captures an image of the target under its FOV. Every image has N number of detectable circles depending on circle grid pattern position respect to the FOV. By running the sequence, a data set is acquired including images from each position the robot was moved.

Second stage of the measurement is preparing the images for data extraction by removing radial distortion from each image. This is where the importance of optimal camera calibration parameters arises. If the camera calibration produces suboptimal values for camera matrix, intrinsic or extrinsic coefficients, radial distortions might not be properly corrected and increases error between the true circle position and measured position.

Third stage of the measurement is data extraction from the undistorted images. Details of the algorithm implementation used for detecting circle center points will not be disclosed due to IPR. In the table 5.1 is an example of the algorithm output from a single image that has a 5x6 pattern of detected circles. The algorithm outputs the robot position coordinates where the image was taken from and the x/y position of each detected circle center point in the image in pixel format. The measurement images in figures 5.8c and 5.8d would both produce similar output as in the example table. This extracted data is stored into a text file where it can be read from in the next stage.

***Figure 5.7.*** *X and Y direction measurement image acquisition*

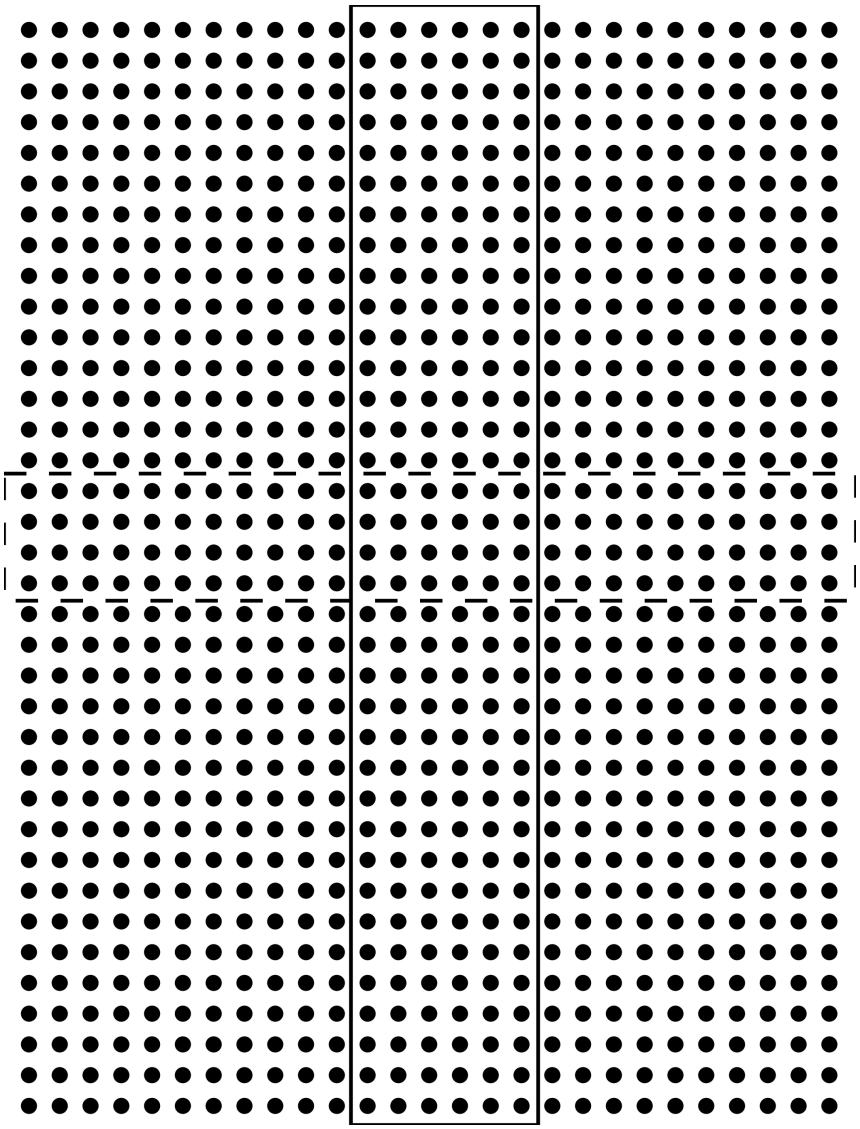

For measuring the robots movement with each increment step and minimizing error caused by deviance in circle detection, the centroid of a grid pattern of detected circles is calculated. The centroid x and y positions are the average value caculated from each detected circle postions with the equations 5.4 and 5.5.

$$centroidXposition = \frac{1}{n} \sum_{circle=1}^{n} circle_{xpos} \tag{5.4}$$

$$centroidYposition = \frac{1}{n} \sum_{circle=1}^{n} circle_{ypos} \tag{5.5}$$

The following subsection 5.7 will give more detail introduction how the circle pattern centroid is used in the measurement.

***Table 5.1.*** *Circle center positions in pixels sorted by X position.*

| Robot coordinates x=80.0, y=48.3, z=107.0 | | | | | | |
|---|---|---|---|---|---|---|
| Row | column1 | | column2 | | column3 | |
| | X px | Y px | X px | Y px | X px | Y px |
| Row1 | 305.079 | 130.783 | 692.472 | 130.899 | 1080.03 | 130.744 |
| Row2 | 305.148 | 523.896 | 692.509 | 524.053 | 1080.11 | 524.016 |
| Row3 | 305.19 | 916.988 | 692.748 | 917.228 | 1080.43 | 917.351 |
| Row4 | 305.611 | 1309.98 | 692.976 | 1310.36 | 1080.75 | 1310.61 |
| Row5 | 305.97 | 1702.84 | 693.434 | 1703.28 | 1081.19 | 1703.58 |
| | column4 | | column5 | | column6 | |
| | X px | Y px | X px | Y px | X px | Y px |
| Row1 | 1467.82 | 130.419 | 1855.94 | 129.972 | 2244.19 | 129.433 |
| Row2 | 1468.04 | 523.718 | 1856.31 | 523.384 | 2244.69 | 522.897 |
| Row3 | 1468.38 | 917.193 | 1856.67 | 916.859 | 2245.19 | 916.398 |
| Row4 | 1468.76 | 1310.47 | 1857.1 | 1310.24 | 2245.65 | 1309.81 |
| Row5 | 1469.28 | 1703.61 | 1857.69 | 1703.5 | 2246.29 | 1703.22 |

## 5.7 Circle pattern tracking

This subsection introduces the method of circle pattern tracking in both x- and y-axis direction. Both measurement directions use the same pattern tracking method. In all images, origin is placed on the top-left hand corner.

- The first captured measurement image is shown in figure 5.8a. A total of 24 circles or a 4x6 grid pattern is detected in the image. The pattern centroid is subpixel position is found at x:1275.8853, y:1002.8684. From this point the robot is commanded to move $1$ mm to its positive y-direction.
- After the robot responses, it has arrived to its new position, second image is captured shown in figure 5.8b. The same circle pattern is detected from the new image and its centroid is at image pixel position x:1274.9510, y:1058.2099. Robot is commanded to do another $1$ mm step.
- In the third captured image 5.8c, the number of detectable circles increases to 30 and two 4x6 circle patterns are detected. In this point, the algorithm calculates the centroid in both patterns. The lower centroid which is marked with solid line is the same pattern as in the first and second image which position is at x:1275.0048, y:1113.5617. The new detected pattern, marked with dotted line has its centroid at x:1274.658, y:720.3208. Up to this point, the algorithm uses the first detected pattern to measure robot movement.
- In the figure 5.8d the algorithm has switched to track the new detected pattern regardless the latter pattern being still detectable.
- Figure 5.8e last row of circles ignored
- Figure 5.8f one pattern detected and position tracked.

***Figure 5.8.*** *Circle pattern tracking in y-direction*

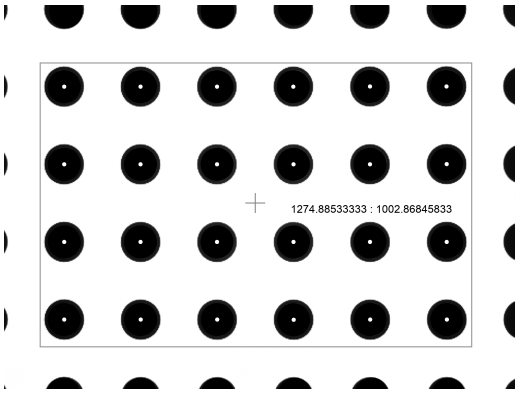


***(a)*** 1st detected pattern position

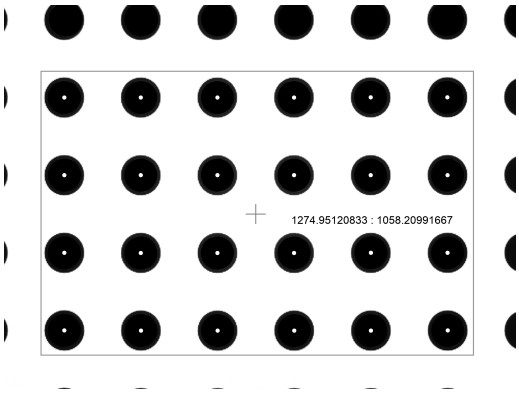


***(b)*** 2nd detected pattern position

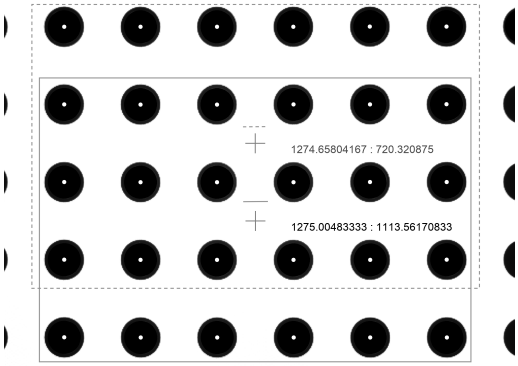


***(c)*** Pattern tracking switch point

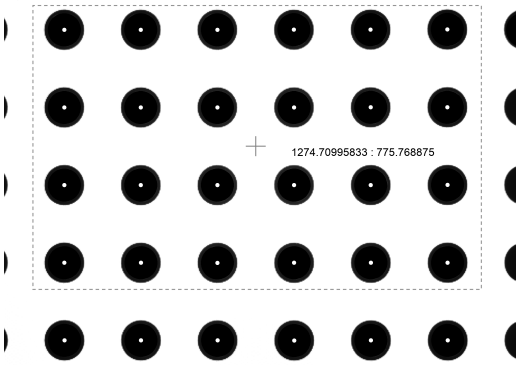


***(d)*** 1st new tracking pattern

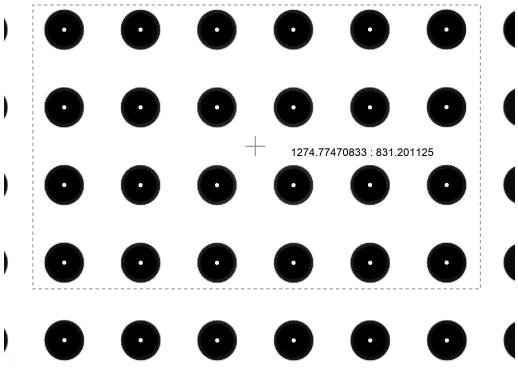


***(e)*** 2nd new tracking pattern

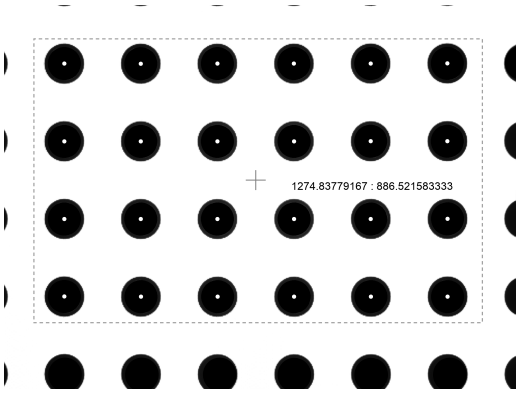


***(f)*** 3rd new tracking pattern

The measurement in x-axis direction is carried out similarly as in y-axis direction. The circle grid pattern size increases from 4x6 to 5x6 when measuring x direction.

- In the measurement image in figure 5.9a a 5x6 circle grid pattern is detected which centroid is at position x:1370.5745px, y:986.7416.
- The next measurement image in figure 5.9b is captured after the robot x-axis moves 1mm step to its positive direction. The grid pattern centroid is now found from coordinates x:1425.073, y:986.6575.
- After another x-axis position increment, two overlapping 5x6 grid patterns are detected shown in figure 5.9c. Both pattern centroids x:1479.5939, y:986.5984 and x:1092.2970, y:986.7467 are saved for further processing. From this point the algorithm begins to track the new

detected pattern and ignores the other even if it detectable in the next images.

- In the figure 5.9d x-axis position has been incremented another 1mm and the new grid pattern centroid has moved to position x:1146.6475, y:986.7143.

***Figure 5.9.*** *Circle pattern tracking in x-direction*

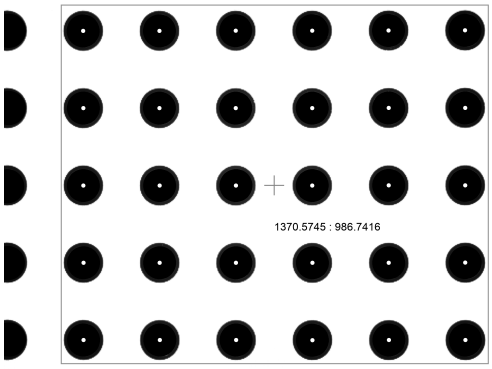


***(a)*** 1st detected pattern position

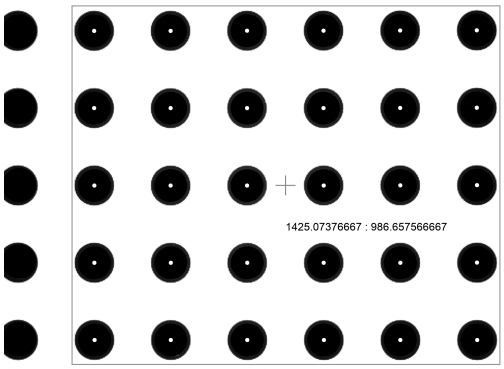


***(b)*** 2nd detected pattern position

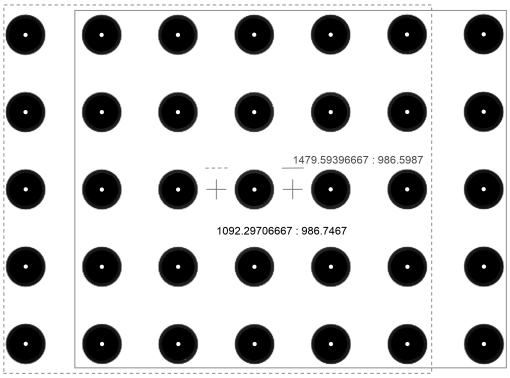


***(c)*** Pattern tracking switch point

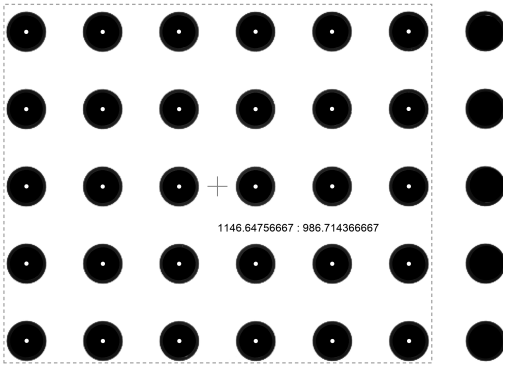


***(d)*** 1st new tracking pattern

This sequence introduced above is repeated through all of the acquired images in both directions.

## 5.8 Positioning error measurement

The robot motion positioning was measured in two ways, linear displacement error along the measured axis and straightness error in the direction orthogonal to the measured axis. Both measurements were calculated from the same acquired images and centroid positions. The error in robot step length was calculated by subtracting measured distance of two sequential centroid positions from the robots reported positions in the location where the images were captured. The measurement was done separately for both axes. For example, when measuring linear displacement error in y-axis positive direction, two sequential grid pattern centroid y positions are subtracted to find the measured step length as shown in the equation 5.9. The centroid coordinates could be e.g. x:1275.8853, y:1002.8684 and x:1274.9510, y:1058.2099 from images captured in robot positions x=80.0, y=50.3, z=107.0 and x=80.0, y=51.3, z=107.0.

$$\begin{aligned} \Delta CYpx &= centroidYpx_{i+1} - centroidYpx_i \\ &= 1058.2099px - 1002.8684px = 55.3415px \end{aligned} \tag{5.6}$$

Where i is the centroid index in the list of all centroids size N. The value $\Delta CY$ is translated to mm by dividing it with the ppmm value show in equation 5.8.

$$\begin{aligned} \Delta\mathrm{CY\,mm} &= \frac{\Delta Y px}{ppmm} \\ &= \frac{55.3415 px}{55.6501 \frac{px}{mm}} = 0.9944\,\mathrm{mm} \end{aligned} \tag{5.7}$$

$$\begin{aligned} YstepError_{i,i+1} &= \Delta\mathrm{CY\,mm} - \Delta\mathrm{RY\,mm} \\ &= 1.0\,\mathrm{mm} - 0.9944\,\mathrm{mm} = -0.005545\,\mathrm{mm} = 5.545\,\mu\mathrm{m} \end{aligned} \tag{5.8}$$

This is repeated through all of the tracked centroids. X-axis direction positioning error is measured and calculated with exact same method and equations, only the X/Y pixel coordinate values change place. The figure 5.10 below shows the measurement results of linear displacement error measurement in y-axis direction and figure 5.11 shows results in x-axis direction.

***Figure 5.10.*** *Y-axis linear displacement error*

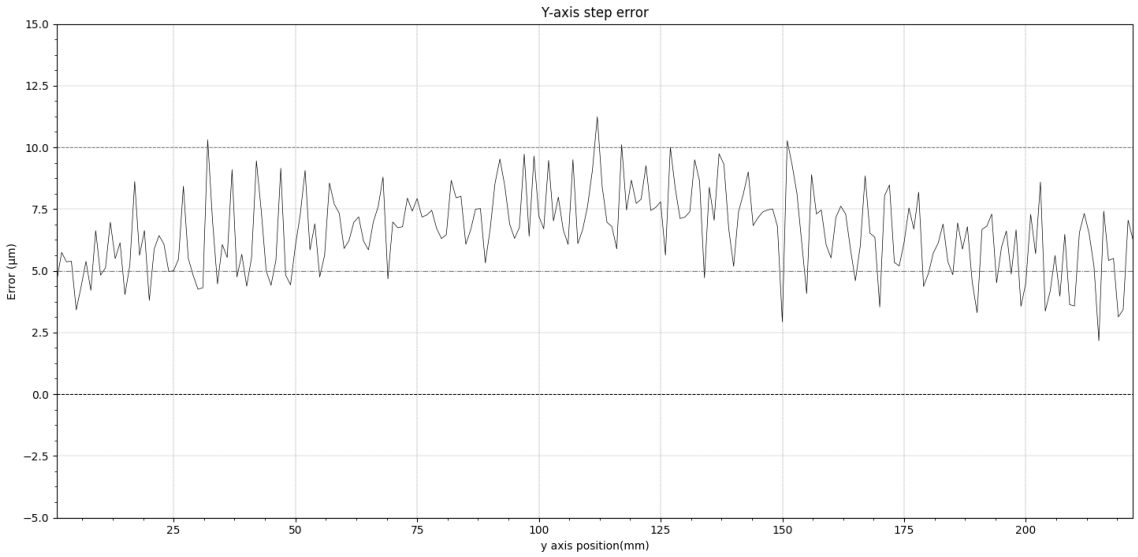


Y-axis straightness error is calculated from the centroid x coordinate. In the below example centroid coordinate $xcentroid_i$ is from figure 5.8a and $xcentroid_{i+1}$ is from figure 5.8b.

$$\begin{aligned} \Delta x &= xcentroid_{i+1} - xcentroid_i \\ &= 1274.8853px - 1274.9512px = 0.0659px \end{aligned} \tag{5.9}$$

The value $\Delta x$ is translated to mm by dividing it with the ppmm value show in equation 5.8.

$$\Delta x = \frac{0.0659 px}{55.6501 \frac{px}{mm}} = 0.00118\,\mathrm{mm} = 1.18\,\mu\mathrm{m}$$

In the y-axis measurement, max deviation was approximately $45\,\mu$m and it was at axis position $220\,$mm. In the y-axis measurement, max deviation was approximately $41\,\mu$m and it was at axis position $140\,$mm.

***Figure 5.11.*** *X-axis linear displacement error*

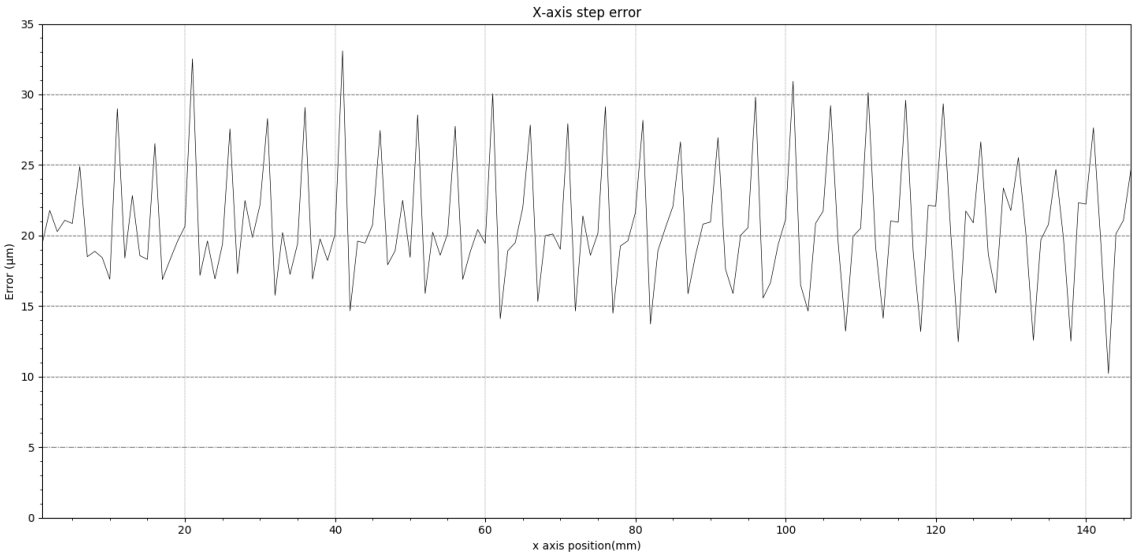


***Figure 5.12.*** *Y-axis straightness error*

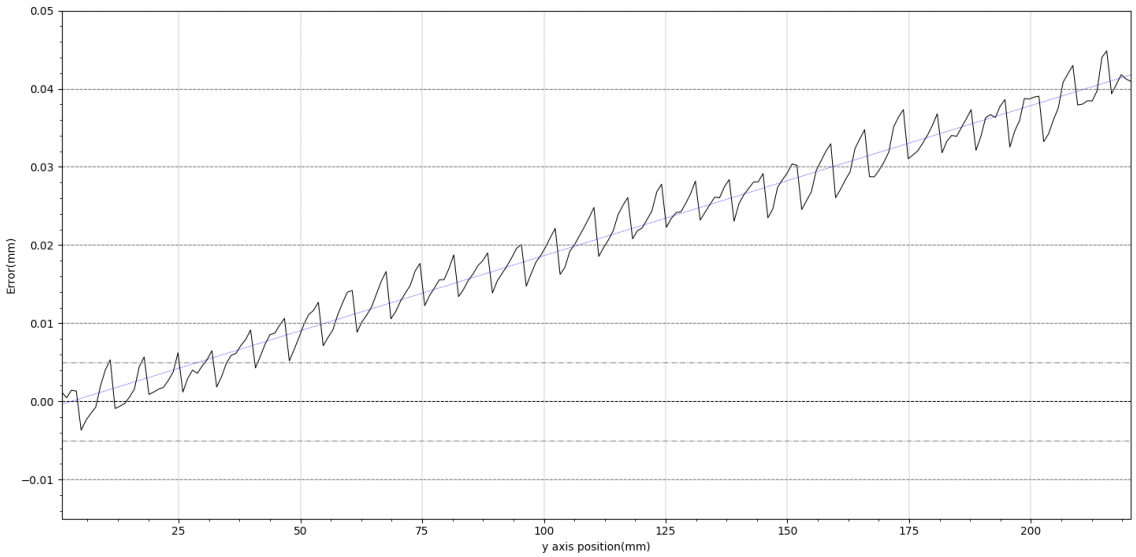


A periodical fluctuation can be seen in both above graphs. This is partially caused by the circle grid mass center point tracking algorithm when it switches between two tracked grid patterns. For instance in x-axis step error measurement, grid pattern tracking begins from the left side of the image when the whole grid pattern is visible. At this point measured step error is lowest and it increases while the grid pattern moves towards right side of the image and peaks at the very last image where the same grid pattern is visible. From this point the algorithm begins to track the next visible pattern from starting again from the left side of the image where step error is at it lowest value. This causes the seen periodical fluctuation in the above graphs. The same happens in y-axis direction measurement when the grid pattern is tracked from top to bottom side of the captured images. Image distortion calibration could have a role in increasing the fluctuation. If the distortion calibration differs from side to side it could have an increasing effect to fluctuation magnitude. Distortion is always greater on the edges of the image than what it is in the middle.

***Figure 5.13.*** *X-axis straightness error*

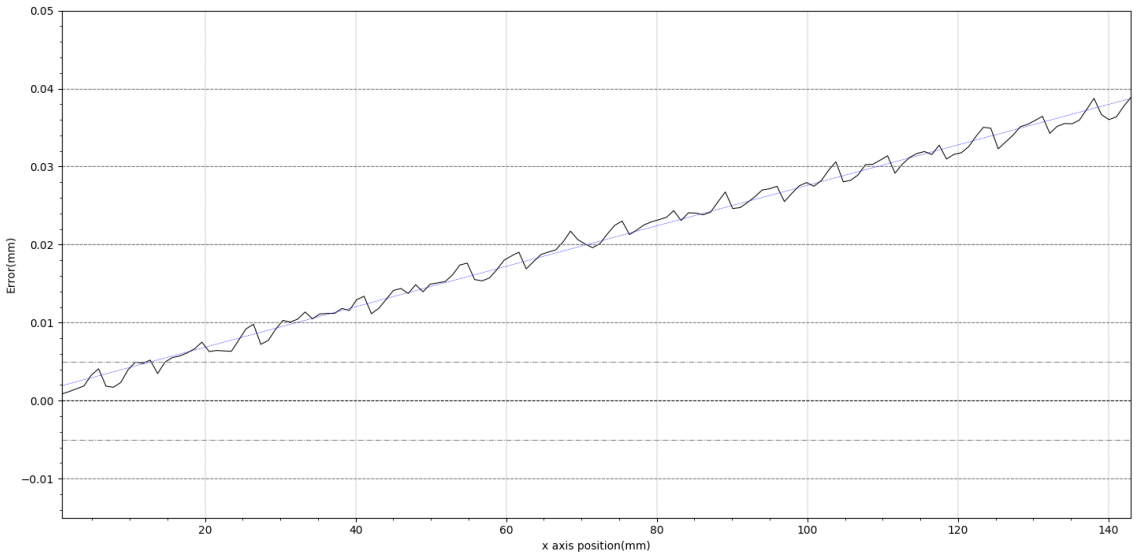


One increasing factor to the seen fluctuation is the fact that the circle grid is not in perpendicular orientation relative to both x and y axis. Also, the cameras orientation to the circle grid is unknown and neither of the angular relations are taken into account in the tracking algorithm. This angular position error can be seen in both figures 5.12 and 5.13. The graphs suggest that the circle grid is tilted in a way that it creates a higher slope in x-axis direction measurement. This could also be causing the larger offset in x-axis direction displacement error measurement which is about $20\,\mu$m and roughly $5\,\mu$m in y-axis linear displacement measurement. As the angular mispositioning is not calculated, it inevitably makes the measurement system more prone to measurement error. Calculating and calibrating the angular relation between grid pattern and camera axis would be the first steps in future development.

Another cause for the seemingly periodical fluctuation could be errors in the robot construction such as ball bearing lead screw manufacturing errors or assembly errors. Some fluctuation is seen also in the validation measurements which were conducted with commercial measurement system. Validation results are presented in the next chapter. Both of these mechanical error sources are in interest to find but the error sources presented above saturate the measurement results making it impossible to distinct neither of these mechanical errors from the results.

# 6 SYSTEM VALIDATION

This chapter goes through the methods utilized for validating the developed measurement system and compares results to a commercial measurement device and to the system developed in the company.

## 6.1 1D validation measurement(Renishaw)

First validation measurement is for step error in the axis direction. This measurement method is based on a linear incremental encoder mounted to the robot z-axis reading data from a grating scale stripe on the robots working area. The linear encoder reading head is attached to the tip of the robot z-axis and it is moved over the grating scale that is glued into a groove on a aluminum plate. The aluminum plate is machined to size that fits the robots working area and it is mounted against alignment pins that prevent misalignment while the robot moves. The robot is moved with 3mm steps along the linear grating scales and reads the recorded incremental signals from the reading-head after each step. Measurement procedure with the encoder is done separately for both x and y axes and the reading-head needs to be re-aligned when changing measurement direction. The manufacturer gives the encoder a +/-$1$ µm accuracy range.

***Figure 6.1.*** *Renishaw RGH22 linear encoder*

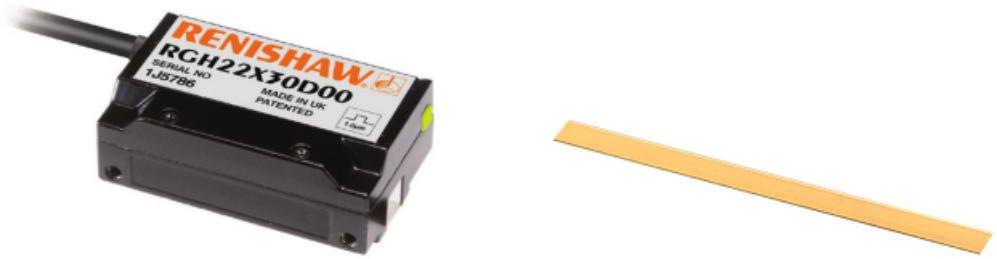


With the incremental measurement method using the Renishaw encoder only linear displacement error is measured. The figure 6.2 shows results from both x and y axis linear displacement error measurement. For y-axis direction, maximum displacement error is roughly $15$ µm at 150mm distance from the measurement starting point. For x-axis direction, maximum displacement error is at 160mm from starting point peaking at roughly $-19$ µm.

As it can be seen from the figure 6.2 the same periodical fluctuation is not evident in the linear displacement validation measurement. Some fluctuation is present especially in the x-axis direction measurement but it is not nearly as large as it was in the results of the developed measurement system. This indicates that the axis has mechanical friction causing the axis motion to vibrate or lag behind the actual commanded motion distance. The magnitude of the fluctuation in these validation measurements are roughly in between 8 to $15$ µm which is much less compared to the first measurement that fluctuated between approximately 15 to $30$ µm. The results do correlate

in the sense that the fluctuation is larger in x-axis than it is in y-axis measurement. Otherwise the results do not correlate as the error in x-axis in the validation measurement is negative which means the axis lags behind the commanded position and in the first measurement results the axis is always ahead of the commanded position. Because the fluctuation is not correlating especially in the y-axis measurement it can be said that most of the fluctuation seen in the results of the developed measurement system is caused by its intrinsic properties and not the measured axis. This also suites the almost constant like offset in both of the first linear displacement measurements. In x-axis the offset was close to $20\,\mu$m and $5\,\mu$m in y-axis measurement. Neither of these offsets are seen in the validation measurements.

***Figure 6.2.*** *x  y axis direction incremental step validation measurement*

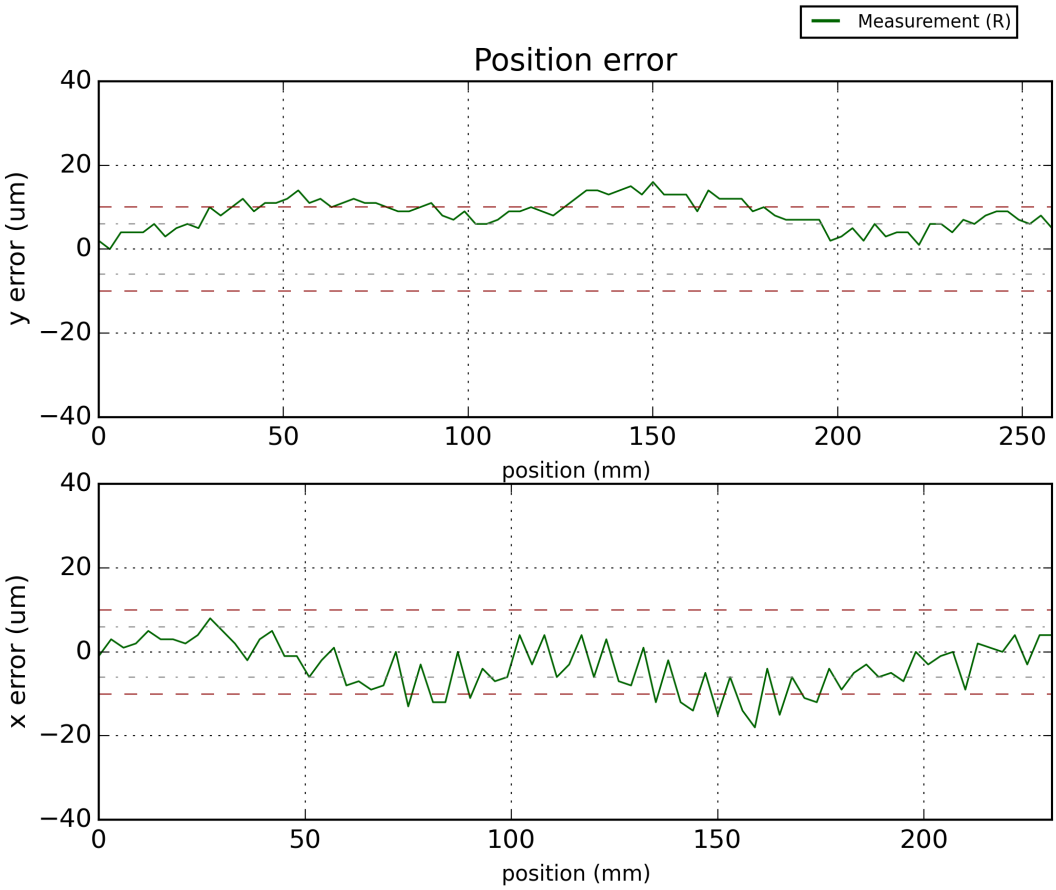

## 6.2 2D validation measurement(Heidenhain)

The two-dimensional validation measurement was done using a Heidenhain KGM182 grid encoder shown in figure 6.3 which was borrowed from production engineering lab at Tampere University of Technology. The KGM measurement device consists of a grid plate with square type graduation embedded into a mounting frame and a read head. It uses an optical encoding to read the grid plate scale, but it has two sensors in the reading head which are phase shifted by 90 degrees. This enables measurement in two directions simultaneously. Like in the 1D measurement, the Heidenhain 2D reading head was mounted to the robot's z-axis and the grid scale was on the robots working area. More information can be found from Heidenhain official web site [8]. The used KGM182 comes with the following accuracy specification:

- Accuracy grade: $\pm 2\,\mu\mathrm{m}$
- Signal period: $4\,\mu$m in both measuring directions
- Measuring step

***Figure 6.3.*** *Heidenhain KGM grid encoder [5]*

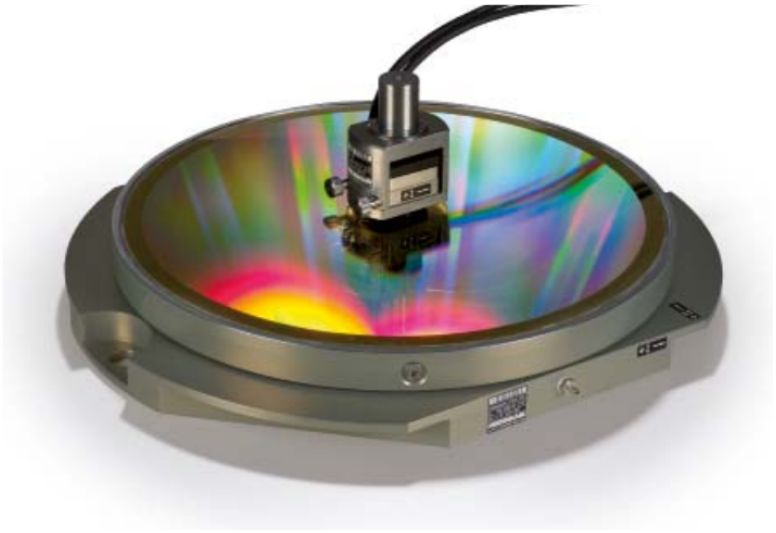

The axis straightness validation measurements with the KGM182 were conducted separately for both axes. Unlike in the SUD the KGM182 measures continuous motion and reads both sensors simultaneously. The robot is moved to a point in its coordinates where the measurement is started. From the starting point the robot is moved $200\,$mm to the positive direction of the measuring axis. The KGM182 records detected motion during the measurement, plots the recorded data and provides a maximum deviation value and the axis position where the largest deviation was found. The two figures 6.4 and 6.5 shows the results for both axes. Both axes were measured four times each with the same starting point and measurement length. All four recorded data sets are plotted to the same figure.

In the x-axis measurement 6.4 max deviation was $8\,\mu$m and it was at axis position $190\,$mm. Some periodical fluctuation is also seen in axis straightness measurement which proves that the axis has mechanical friction causing motion error. Otherwise the x-axis is almost ideal as it only has a very small deviation from optimal path. The results of developed measurement system has two main components, periodical fluctuation and the linearly increasing error. Neither of these error components are seen in the straightness error validation measurements in x-axis direction. This

proves that the linear error in the straightness measurement is not caused by the errors in robot construction but it is caused by the circle grid angular mispositioning.

***Figure 6.4.*** *x-axis straightness error*

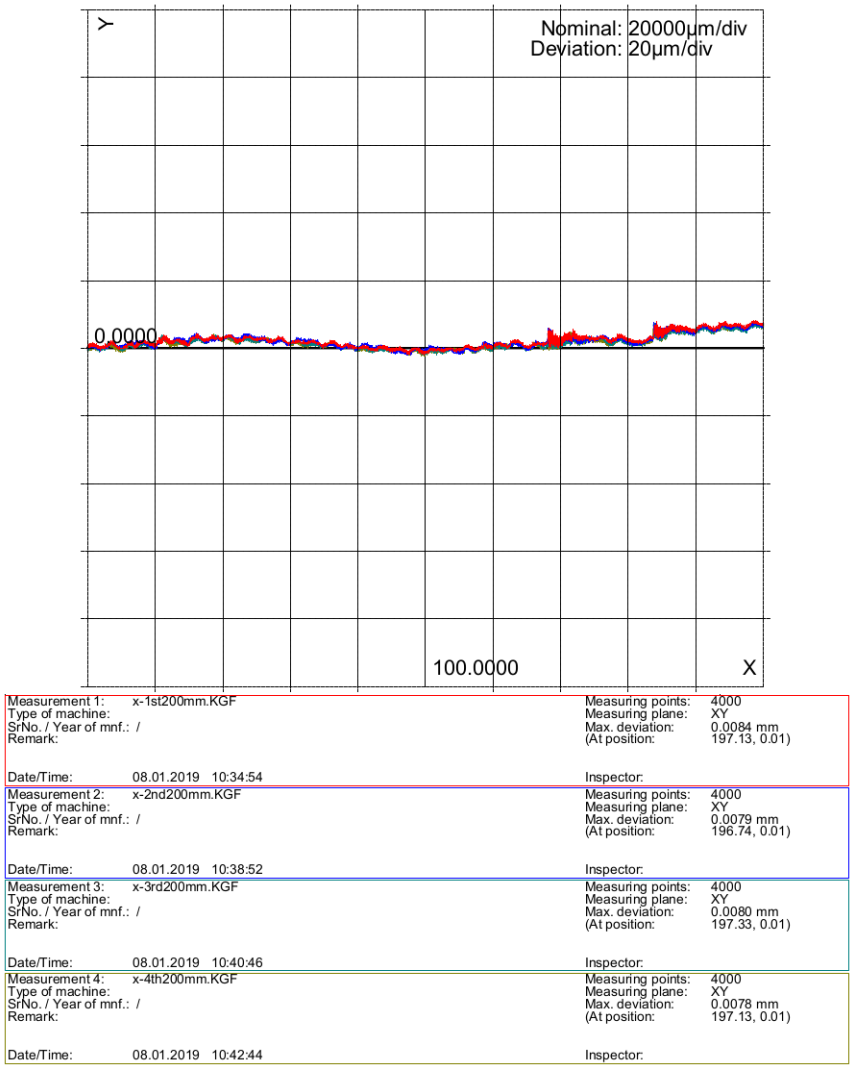


In the y-axis measurement, max deviation was $28.1$ µm and it was at axis position $197.06$ mm. A better correlation can be seen in the y-axis direction straightness measurements. A periodical and linear error is present in both measurements although the magnitude of both error components are far less in the validation measurement results. The periodical fluctuation in figure 6.5 is most likely caused by the manufacturing and assembly errors in the y-axis ball bearing lead screw. The fluctuation occurs about 3 time within every 20mm travelled. This suggests that the lead screw is bent in a way that it causes the axis to speed up or slowdown in every 6-7mm period of distance travelled. The fluctuation is larger in the beginning 40mm distance and settles to a lower amplitude for the rest of the measured travel unlike in the results of the developed system where the fluctuation remains more constant from start to end of measured travel distance. It can also be clearly seen from validation and the initial measurement that the maximum error is almost double peaking at roughly $40$ µm with the developed system.

***Figure 6.5.*** *y-axis straightness error*

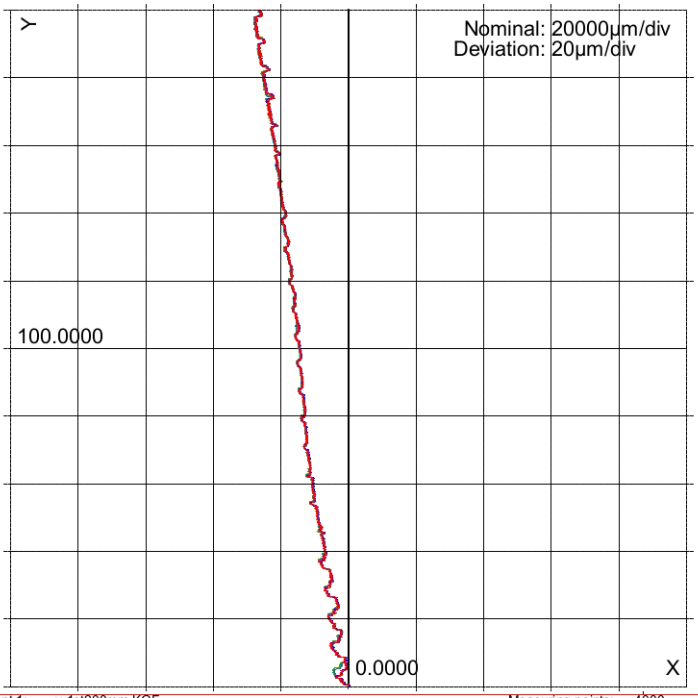


| | | | |
|---|---|---|---|
| Measurement 1: | y-1st200mm.KGF | Measuring points: | 4000 |
| Type of machine: | | Measuring plane: | XY |
| SrNo. / Year of mnf.: | / | Max. deviation: | 0.0277 mm |
| Remark: | | (At position: | -0.03, 196.96) |
| Date/Time: | 08.01.2019 10:48:37 | Inspector: | |
| Measurement 2: | y-2nd200mm.KGF | Measuring points: | 4000 |
| Type of machine: | | Measuring plane: | XY |
| SrNo. / Year of mnf.: | / | Max. deviation: | 0.0277 mm |
| Remark: | | (At position: | -0.03, 196.26) |
| Date/Time: | 08.01.2019 10:50:16 | Inspector: | |
| Measurement 3: | y-3rd200mm.KGF | Measuring points: | 4000 |
| Type of machine: | | Measuring plane: | XY |
| SrNo. / Year of mnf.: | / | Max. deviation: | 0.0281 mm |
| Remark: | | (At position: | -0.03, 196.35) |
| Date/Time: | 08.01.2019 10:52:12 | Inspector: | |
| Measurement 4: | y-4th200mm.KGF | Measuring points: | 4000 |
| Type of machine: | | Measuring plane: | XY |
| SrNo. / Year of mnf.: | / | Max. deviation: | 0.0281 mm |
| Remark: | | (At position: | -0.03, 197.06) |
| Date/Time: | 08.01.2019 10:55:00 | Inspector: | |

# 7 CONCLUSION

The goal of this thesis was to develop a measurement system for quantifying linear axis positioning error of a cartesian robot within its XY-plane. To create a baseline for the development requirements a literature study of cartesian robot linear axis positioning error sources and measurement uncertainty were conducted. A selection of technologies was predefined which were to be evaluated for suitability to be used in the measurement system. The evaluation was conducted using a scoring system based on requirements and constrains set for the technology and for characteristics of the system that was to be developed. After conducting the technology evaluation, a camera-based solution was found to be the most suitable technology to begin developing the measurement system.

The developed system is a proof-of-concept that a measurement system based on camera technology and imaging algorithms can be used for measuring robot positioning error. The results of the developed measurement system were validated using commercial measurement systems. Proven by the validation results, the developed measurement system has too much uncertainty within its results to reliably quantify positioning error and to fulfill the robot applications high accuracy demands. The developed system does fulfill the requirements for integrability, cost efficiency and x/y-plane measurement. With possible future development the system accuracy performance can be improved to match the requirements.

To increase the measurement system accuracy the camera should have a sensor with higher resolution and optics should be changed to decrease the area of field of view to gain higher ppmm value. The area of FOV can be decreased with longer focal length optics. This will increase the ppmm value and result in a better measurement accuracy. Changing the lens focal length and decreasing FOV area will require the measurement target to be redesigned to have much smaller circle diameter. The alignment offset between the measurement target and camera sensor should be taken into account and calibrated to minimize uncertainty caused by angle offset.

# REFERENCES


[1] *A Beginner's Guide to Uncertainty of Measurement*. Tech. Report 2. United Kingdom: Centre for Basic, Thermal and Length Metrology, National Physical Laboratory(NPL), 1999.

[2] *An Introduction to Laser Triangulation Sensors*. AZO sensors, webpage. 2014. URL: https://www.azosensors.com/article.aspx?ArticleID=523 (visited on 08/28/2014).

[3] S. Dejima, W. Gao, H. Shimizu, S. Kiyono, and Y. Tomita. Precision positioning of a five degree-of-freedom planar motion stage. In: *Mechatronics* 15 (2005), 969–987. DOI: 10.1016/j.mechatronics.2005.03.002. URL: https://ac.els-cdn.com/S0957415805000589/1-s2.0-S0957415805000589-main.pdf?_tid=f6ba83a1-8086-40bd-94cd-fed2111c5e0f&acdnat=1527147230_13509203a87d3289b9955bf236b431bf.

[4] D. Dornfeld and D.-E. Lee. *Precision Manufacturing*. 233 Spring Street, New York, NY 10013, USA: Springer Science+Business Media, 2008.

[5] *Encoders For Machine Tool Inspection and Acceptance Testing*. Datasheet. Heidenhain corporation, 2017. URL: https://www.heidenhain.com/fileadmin/pdb/media/img/208871-29_Measuring_Devices_For_Machine_Tool_Inspection_and_Acceptance_Testing_01.pdf.

[6] A. J. Fleming and K. K. Leang. *Design, Modeling and Control of Nanopositioning Systems*. Springer International Publishing Switzerland, 2014.

[7] B. Greenway. Robot accuracy. In: *Industrial Robot: An International Journal* 27.4 (2000), 257–265. DOI: 10.1108/01439910010372136. URL: https://doi.org/10.1108/01439910010372136.

[8] *Heidenhain Grid Encoder*. Heidenhain, webpage. URL: https://www.heidenhain.com/en_US/products/grid-encoder/kgm/.

[9] *Interferometry explained*. Renishaw, webpage. URL: http://www.renishaw.com/en/interferometry-explained--7854.

[10] *JCGM 200:2008 International vocabulary of metrology — Basic and general concepts and associated terms (VIM)*. Tech. rep. Joint Committee for Guides in Metrology, 2008.

[11] R. Leach. *Fundamental Principles of Engineering Nanometrology*. Elsevier Inc, 2014.

[12] *Leica AT930 Absolute interferometer*. Hexagon, webpage. 2019. URL: https://www.hexagonmi.com/products/laser-tracker-systems/leica-absolute-tracker-at930 (visited on 12/09/2019).

[13] C. Ratcliffe and B. Ratcliffe. *Doubt-Free Uncertainty In Measurement*. Springer International Publishing Switzerland, 2015.

[14] E. S. F. dos Santos, W. B. Xavier, R. N. Rodrigues, S. S. da C. Botelho, and A. V. Werhli. Vision Based Measurement applied to Industrial Instrumentation. In: *IFAC PapersOnLine* 50.1 (2017), 788–793. URL: https://doi.org/10.1016/j.ifacol.2017.08.509.

[15] M. Slamani, A. Nubiola, and I. A. Bonev. Assesment of the Positioning Performance of an Industrial Robot. In: *Industrial Robot* 39.1 (2012), 57–68.

[16] G. T. Smith. *Machine Tool Metrology, An Industrial Handbook*. Springer International Publishing Switzerland, 2016.

[17] *Technical Explanation for Displacement Sensors and Measurement Sensors*. Tech. Report. Omron Industrial Automation. URL: http://www.ia.omron.com/data_pdf/guide/56/displacemente_linewidth_tg_e_2_1.pdf.

[18] *Test code for machine tools — Geometric accuracy of machines operating under no-load or quasi-static conditions, part 1*. ISO 230-1:2012(E). Switzerland: International Organization for Standardization, 2012.

[19] *THE INTERNATIONAL SYSTEM OF UNITS (SI)*. NIST special publication 330. United States of America: National Institute of Standars and Technology, 2008.

[20] T. V. Zavrazhina. A Control for Spatial Motions of a Robot in a Rectangular Cartesian Coordinate System. In: *Journal of Computer and Systems Sciences International*. Vol. 45. Kiev, Ukraine: Pleiades Publishing, Inc, 2006, 2005, 658 –670. URL: https://link-springer-com.libproxy.tut.fi/content/pdf/10.1134%2FS1064230706040174.pdf.